Article

#-Conjugate Fluorophore-tagged and Enzyme-responsive L-Amino acid Polymer Nano-carrier and their Colour-tunable Intracellular FRET Probe in Cancer Cells

Sonashree Saxena, and Manickam Jayakannan

Biomacromolecules, **Just Accepted Manuscript** • DOI: 10.1021/acs.biomac.7b00710 • Publication Date (Web): 12 Jul 2017

ACS Publications

Biomacromolecules is published by the American Chemical Society. 1155 Sixteenth Street N.W., Washington, DC 20036

π-Conjugate Fluorophore-tagged and Enzyme-responsive L-Amino acid Polymer Nano-carrier and their Colour-tunable Intracellular FRET Probe in Cancer Cells

Sonashree Saxena and Manickam Jayakannan*[1]

Department of Chemistry, Indian Institute of Science Education and Research (IISER) Pune, Dr. Homi Bhabha Road, Pune 411008, Maharashtra, INDIA

Corresponding Author: M. Jayakannan (e-mail: jayakannan@iiserpune.ac.in)

Keywords: L-Amino acid Polymers, FRET Probes, Bio-imaging, π-conjugated polymers, Enzyme-responsiveness and Biodegradation.

Abstract

The present investigation accounts one of the first example of enzyme-responsive and π-conjugate-tagged L-amino acid amphiphilic polymer and their fluorescence resonance energy transfer (FRET) probes for colour-tunable intracellular bio-imaging in cancer cells. Melt polymerizable oligo-phenylenevinylene (OPV) π-conjugated diol was tailor-made and subjected to thermo-selective melt transesterification reaction with multi-functional L-aspartic acid monomer to yield OPV-tagged amphiphilic luminescent polyesters. These amphiphilic polyesters self-assembled through strong aromatic π-π stacking and hydrophilic/hydrophobic non-covalent forces into < 200 nm size blue-luminescent nanoparticles in aqueous medium. The OPV-tagged polymer nanoparticles served as FRET donor and encapsulated water insoluble Nile Red (NR) fluorophore as a FRET acceptor. Detail photophysical studies revealed that both the OPV and NR were confined within Förster distance in the polymer nano-container and the nano-domains provided appropriate

[1] E-mail: jayakannan@iiserpune.ac.in

geometry for efficient excitation energy transfer from OPV to NR. Cytotoxicity studies in breast cancer (MCF 7), cervical cancer (HeLa) and normal (Wild-type MEF) cell lines revealed that both the nascent luminescent OPV nanoparticles and OPV-NR FRET probes were non-toxic to cells up to 100 μg/mL. Confocal microscope images confirmed the efficient transportation of polymer and FRET probes across the cell membranes and their preferable accumulation in the cytoplasm of the cells. Lysosomal tracker assisted live cell imaging provided direct evidence for the localization of the polymer nanoparticles at the lysosomal compartments in the cytoplasm. *In vitro* enzyme-responsive studies revealed that the aliphatic polyester backbone in the polymer nanoparticles was readily biodegradable by lysosomal enzymes like esterase, chymotrypsin, trypsin and also redox GSH species in the cytoplasm. Selective photoexcitation in confocal microscope exhibited bright OPV blue-luminescence and strong red-emission from NR followed by the excitation energy transfer and occurrence of FRET process at the intracellular environment in cancer cell lines. Both the polymer design and the biodegradable polymer FRET concept are completely new; thus, the present approach opens up new platform of research opportunities for natural L-amino acid based luminescent polymer probes for colour-tunable bio-imaging in cancer cells.

Introduction

Fluorescent-probe tagged amphiphilic polymers are emerging as dual-function nano-carriers to deliver anticancer drugs/genes to cancer tissues as well as luminescent biomarkers in cancer diagnosis.[1-7] Förster or fluorescence resonance energy transfer (FRET) is one of the most powerful non-invasive fluorescence probe[8] and it functions on the basis of selective photoexcitation energy transfer from donor to acceptor chromophores within the nano-confinement of ≤ 50 Å.[9] FRET technique is explored for real-time tumor-imaging,[10-11] drug release kinetics,[12-13] studying the self-assembly of amphiphilic block copolymers,[14] protein folding under physiological conditions,[15-16] quadruplex-to-duplex transitions in DNA,[17] molecular interactions at the mammalian cell surfaces,[18-20] two-photon imaging in cancers,[21-22] and sensing of bilirubin in human serum,[23] etc. In the last 2-3 decades, significant advancements made in the area of conducting polymers for optoelectronic devices has opened new arena of opportunities for water soluble cationic π-conjugated polymers as luminescent bio-probes.[2, 24] Cationic and water soluble polyfluorenes are some of the most important π-conjugated polymers reported for FRET applications.[25-32] Polyacrylates based random and block copolymers having optical chromophores in the side chains were also reported for FRET applications.[12,14] Unfortunately, the non-biodegradability of the rigid C-C backbone in the π-conjugated polymers and acrylates are still one of the major challenges to overcome for their wide applicability in biomedical research. New synthetic approaches towards the development of luminescent π-conjugated chromophores in combination with biodegradable polymer backbone would provide new opportunities for biodegradable-cum-luminescent π-conjugated nano-scaffolds in a single system.[33-34] Further, this new design would also allow simultaneous tracing of the cellular uptake of the luminescent nano-carriers and their responsiveness to digestion at the intracellular regions in cancer cells. Unfortunately, up to our knowledge, no efforts have been taken until now to develop biodegradable luminescent polymers and their FRET probes which are very crucial for long-term application in cancer treatment.

L-Amino acid based polymers are important biomaterials due to the large abundance of monomer resources in nature along with their excellent bio-availability and biodegradability under physiological conditions.[35] Polypeptides,[36] PEG-containing di-and tri-block polypeptide block copolymers,[37] poly(ester-amides),[38-41] poly(α-hydroxy acids),[42] polycarbonates,[43-47] and poly(disulfide)s[48-49] were developed from L-amino acid resources and they were employed for drug and gene delivery. From our laboratory, we reported

solvent free melt polycondensation approach for L-amino acid resources to synthesize wide range of linear poly(ester-urethane)s,[50-51] hyperbranched poly(ester-urethane)s,[52] disulfide containing polyesters[53] and functional aliphatic polyesters.[54] Enzyme and pH responsive L-aspartic amphiphilic polyester[55] and L-tyrosine poly(ester-urethane)[56] were also developed for delivery of multiple anticancer drugs. Unfortunately, most of these L-amino acid polymers were non-luminescent in nature; thus, their cellular uptake and enzymatic biodegradation at the intracellular compartments could not be studied by fluorescence techniques. To accomplish this goal, here we report a new polymer design by combining the π-conjugated fluorophore and enzyme-responsive L-amino acid based aliphatic polyesters. Our expertise in the area of melt polymerization synthetic methodologies for L-amino acid polymers and π-conjugated materials in bio-imaging[57-59] provided a unique opportunity to combine these two areas to construct a novel *enzyme-responsive* FRET probe concept. Aliphatic esters are one of the most sought after enzyme-responsive chemical stimuli in pro-drug industry (more than 49 %); thus, L-aspartic acid based aliphatic polyester was chosen as the enzyme-biodegradable backbone.[60] A new melt polymerisable π-conjugated oligo-phenylenevinylene (OPV) diol was tailor-made[33] and subjected to thermo-selective melt transesterification (developed in our lab) to accomplish the targeted polymer structures. This new enzyme-responsive and biodegradable FRET probe concept is shown in figure 1.

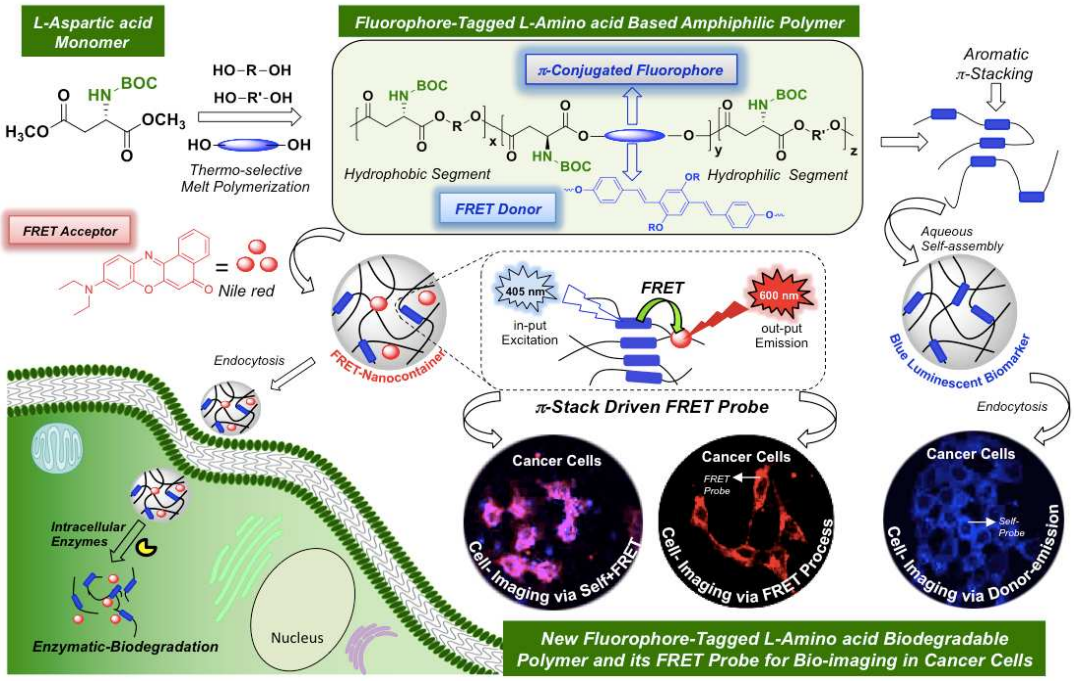

Figure 1. *Development of enzyme-responsive π-conjugated fluorophore-tagged L-aspartic acid polyester and its FRET probe for bio-imaging at the intracellular level.*

The present investigation emphasises the design of π-conjugate-tagged L-amino acid based polymer luminescent probes in order to study the functioning of the FRET probe by detailed photophysical techniques, and also to demonstrate their intracellular bio-imaging capabilities in cancer cells. The new polymer luminescent probe has the following in-built features: (i) amphiphilicity in the L-aspartic polyester backbone and blue-luminescent characteristics accomplished by choosing appropriate OPV-diol along with hydrophilic/hydrophobic segments , (ii) the strong aromatic π-stacking interaction among the OPV chromophores produced π-aggregated species which acted as blue-luminescent self-probe as well as FRET donor, (iii) the encapsulation of water insoluble Nile Red (FRET acceptor) in the polymer nanoparticle cavity enabled the formation of OPV-NR FRET donor-acceptor pair, (iv) the FRET probe was found to be enzymatically-biodegradable, non-toxic and readily taken up by cancer cells, and (v) selective photoexcitation experiments in confocal microscope facilitated the colour-tunable imaging with blue, red and magenta emission at the intracellular level in breast cancer (MCF 7), cervical cancer (HeLa) and normal embryonic fibroblast (WT-MEF) cell lines. Upon exposure to lysosomal-enzymes, the polymer nano-scaffold underwent biodegradation to excrete the polymer donor and NR acceptor molecules once the probing action was done at the cellular level. Detailed photophysical techniques such as absorption, emission and time-correlated fluorescence decay dynamic experiments were carried out to determine the Förster distance and to confirm the occurrence of FRET process between the OPV donor and NR acceptor. The FRET probe was employed as colour-tunable biomarker and the proof-of-concept was demonstrated *in vitro* at the intracellular compartments of cells. The present investigation opens up new platform of research activities for the development of biodegradable L-amino acid polymer FRET probes which is yet to be explored in the literature.

Experimental Section

Materials: L-Aspartic acid, 1,12-dodecandiol (DD) , hydroquinone, triethylphosphite, 4-hydroxybenzaldehyde, KOtBu (1.0 M in THF), triethylene glycol (TEG), ethylhexyl bromide, titanium tetrabutoxide ($Ti(OBu)_4$), 2-chloroethanol, Nile Red, potassium iodide, curcumin, horse liver esterase enzyme, MTT crystal (tetrazolium salt: 3-(4,5-dimethylthiazolyl)-2,5-diphenyltetrazolium bromide), fluoromount^{TM} aqueous mounting medium , 4′,6-diamidino-2-phenylindole (DAPI), chymotrypsin, papain and glutathione (GSH) were purchased from sigma aldrich chemicals. Trypsin phosphate versene glucose

(TPVG) solution 1X was purchased from Hi Media. Mammalian breast cancer MCF 7, cervical cancer (HeLa) and normal wild type-MEF cells were maintained in a phenol red containing Gibco DMEM with 10% (v/v) fetal bovine serum (FBS) and 1% (v/v) penicillin–streptomycin. 96-well and 6-well flat bottomed plastic plates were obtained from Costar and Lab TEK 8 well cover glass chamber were obtained from Nunc Lab Tek. Lysotracker® Green DND-26 was obtained from Cell Signalling Technologies (CST). Paraformaldehyde, HBr in glacial acetic acid, potassium carbonate, potassium sulphate, potassium hydroxide, sodium bicarbonate were purchased locally. HPLC THF and HPLC DMSO were obtained from Spectrochem Laboratories. Thionyl chloride, methanol, THF, ethyl acetate, petroleum ether, DMF, DMSO and other solvents were purchased locally and purified before use. All the other reagents were purchased from Sigma Aldrich and used as such.

General Procedure: Primary characterization of synthesized polymers was done using ^{1}H-NMR and ^{13}C-NMR 400 and 100 MHz JEOL NMR Spectrophotometer respectively. $CDCl_3$ was used as a reference solvent and TMS was used as internal standard. Mass of the compounds synthesised were determined using Applied Bio system 4800 PLUS matrix-assisted laser desorption/ionization (MALDI)TOF/TOF analyzer and Gas Chromatography-Mass Spectrometry GC 2010 Shimadzu. Thermogravimetric analysis (TGA) was used to measure the thermal stability of the polymers using PerkinElmer thermal analyzer STA 6000 model under nitrogen environment at a heating rate of 10°C/min. Indium standards were used to calibrate the system before use. TA Q20 Differential Scanning Calorimetry (DSC) was used to obtain the DSC curves of polymers at a heating and cooling rate of 10°C/min. In order to remove thermal prehistory from samples the polymers were preheated to melt before recording their thermograms. The molecular weights of the polymer were obtained in THF using Gel permeation chromatographic (GPC) analysis with Viscotek VE 1122 pump, Viscotek VE 3580 RI detector and Viscotek VE 3210 UV/VIS detector with respect to polystyrene standards. Dynamic Light Scattering (DLS) from Malvern Instruments was used for estimating the size of polymer nanoparticles suspended in water. Microscopic images were obtained using Zeiss Ultra Plus scanning electron microscope for field emission scanning electron microscopy (FE-SEM) images, Veeco Nanoscope IV instrument in tapping mode for Atomic Force Microscopy (AFM) images and LSM710 confocal microscope for confocal images. Perkin Elmer Lambda 45 UV-vis spectrophotometer and SPEX Fluorolog HORIBA JOBIN VYON fluorescence spectrophotometer (with double gating 0.22 m Spex 1680 monochromator and excitation source as 450 W Xe lamp) were employed to obtain

absorption spectra and emission spectra for dye and drug loaded polymer in aqueous media. Varioskan FLASH instrument was used for measuring absorbance in MTT experiments.

Synthesis of 1,4-Bis(2-ethylhexyloxy) benzene (1): Hydroquinone (15.0 g, 0.14 mol) and potassium hydroxide (30.6 g, 0.55 mol) were dissolved in dry DMSO (100 mL) and heated to 80 °C for 30 minutes. This was followed by dropwise addition of 2-ethylhexyl bromide (53.2 mL, 0.30 mol) and the reaction mixture was refluxed at 80 °C for 48 h under nitrogen atmosphere. The reaction mixture was cooled, DMSO was distilled off under vacuum, and the product was extracted in DCM using washing with 5% NaOH. The organic layer was dried over anhydrous Na_2SO_4 and solvent was evaporated to obtain brown solid mass. It was further purified using silica gel column using pet ether system. Yield = 30.0 g (66 %). ^{1}H NMR ($CDCl_3$, 400 MHz) δppm: 6.85 ppm (s, 4H, aromatic protons), 3.81 (m, 4H, -OC**H**$_2$), 1.72 (m, 2H, OCH_2C**H**), 1.51-1.36 (m, 16H, aliphatic protons), and 0.97-.92 (t, 12 H, C**H**$_3$). ^{13}C NMR ($CDCl_3$, 100 MHz) δ ppm: 153.51, 115.44, 71.28, 39.54, 30.61, 29.17, 23.93, 23.16, 14.19, 11.19. FT-IR (cm^{-1}): 2957, 2924, 2864, 1506, 1464, 1382, 1283, 1222, 1109, 1038. MALDI-TOF-MS: m/z calculated for $C_{22}H_{38}O_2$: 334.54 and found 357.30 [$M^+ + Na^+$] and 373.28 [$M^+ + K^+$].

Synthesis of 1,4-Bis(bromomethyl)-2,5-bis-(2-ethylhexyloxy) (2): Compound **1** (10.0 g, 0.03 mol) was dissolved in glacial acetic acid (30.0 mL), and paraformaldehyde (3.60 g, 0.12 mol) was added to this solution at 25 °C. The reaction mixture was stirred for 15 min followed by drop wise addition of HBr in glacial acetic acid (30.0 mL, 0.06 mol). The reaction mixture was heated to 80 °C and was refluxed for 6 h. The reaction mixture was cooled to 25 °C and carefully poured into large amount of water. A white precipitate was observed and this product was re-crystallized three times in hot isopropanol to yield pure product. Yield: 9.0 g (58 %). ^{1}H NMR ($CDCl_3$, 400 MHz) δ ppm: 6.86 ppm (s, 2H, aromatic protons), 4.54 (s, 4H, -C**H**$_2$Br), 3.89 (d, 4H, OC**H$_2$**), 1.79-1.74 (m, 2H, -OCH_2C**H**), 1.51-1.34 (m, 22H, aliphatic protons) and 0.98-.90 (m, 12 H, C**H**$_3$). ^{13}C NMR ($CdCl_3$, 100 MHz) δppm: 150.79, 127.45, 114.31, 71.01, 39.68, 30.72, 29.19, 28.84, 24.10, 23.14, 14.17, 11.32 . FT-IR (cm^{-1}): 2960, 2928, 2867, 1505, 1466, 1442, 1307, 1221, 1120, 1085, 1030 and 911.

Synthesis of Tetraethyl(2,5-bis(2-ethylhexyloxy)-1,4-phenylene)bis(methylene) diphosphonate (3): Compound **2** (4.0 g, 7.7 mmol) and triethylphosphite (2.90 mL, 17.0 mmol) were refluxed at 150 °C for 10 h. The excess of triethylphosphite was removed by

vacuum distillation and the product was purified using silica gel using ethyl acetate and pet ether (20% v/v). Yield = 4.67 g (96 %).^{1}H NMR ($CDCl_3$, 400 MHz) δ ppm: 6.93 ppm (s, 2H, Ar-**H**), 4.05-3.96 (m, 8H, -POC**H**$_2$CH$_3$), 3.81-3.79 (m, 4H, OC**H$_2$**), 3.24-3.19 (d, 4H, C**H**$_2$P), 1.72-1.69 (m, 2H, -OCH$_2$C**H**), 1.46-1.31 (m, 16H, aliphatic protons), 1.23 (t, 12H, -PCH$_2$C**H**$_3$) and 0.94-0.90 (m, 12 H, C**H**$_3$). ^{13}C NMR ($CDCl_3$, 100 MHz) δ ppm: 150.50, 119.38, 114.75, 71.24, 61.91, 39.74, 30.67, 29.18, 26.91, 23.98, 23.11, 16.42, 14.13, 11.22. FTIR (cm^{-1}): 2960, 2926, 2867, 1648, 1509, 1466, 1391, 1247, 1210, 1163, 1097, 1022, 955. MALDI-TOF-MS: m/z calculated for $C_{32}H_{60}O_8P_2$: 634.77 and found 657.47 [$M^+ + Na^+$] and 673.45 [$M^+ + K^+$].

Synthesis of 4-(2-Hydroxyethoxy) benzaldehyde (4): 4-Hydroxybenzaldehyde (5.0 g, 0.04 mol), potassium carbonate (14.14 g, 0.10 mol) was taken in dry DMF (60.0 mL) and heated at 80 °C for 10 min and further stirred for 1 h. 2-Bromoethanol (4.35 mL, 0.06mol), catalytic amount of KI were added and reaction was refluxed for 48 h. DMF was removed from the reaction mixture by vacuum distillation, and the product was extracted in DCM. The crude product was further purified in silica gel using pet ether and ethyl acetate system (4:1, v/v). Yield: 2.7 g (40 %). ^{1}H NMR ($CDCl_3$, 400 MHz) δ ppm: 9.89 (s, 1H, C**H**O), 7.84 (d, 2H, Ar-**H**), 7.03 (d, 2H, Ar-**H**), 4.16 (t, 2H, ArOC**H**$_2$), and 4.01 (t, 2H, C**H**$_2$OH). ^{13}C NMR ($CDCl_3$, 100 MHz) δppm: 190.99, 163.77, 132.14, 130.27, 114.90, 69.64, 61.23. FTIR (cm^{-1}): 3395, 2939, 2873, 1673, 1597, 1508, 1395, 1253, 1216, 1158, 1078. GC-MS m/z calculated for $C_9H_{10}O_3$= 166.17 and found 166.

Synthesis of Hydroxyl functionalized oilgo-phenylenevinylene (HO-OPV-OH): Compound **3** (4.0 g, 6.30 mmol) and compound **4** (2.2 g, 13.0 mmol) were taken in dry tetrahydrofuran (60.0 mL) and the contents were cooled to 4°C under nitrogen atmosphere. Potassium t-butoxide (37.0 mL in THF, 6.30 mmol) was added and the reaction was continued for 12 h with stirring at 25 °C. THF was evaporated and the content was added to water, extracted using chloroform. It was dried over Na_2SO_4 , solvent was removed and the product was purified in silica gel column using pet ether and ethyl acetate system (50 % v/v). Yield = 2.1 g (50 %) ^{1}H NMR ($CDCl_3$, 400 MHz) δppm: 7.48-7.46 ppm (d, 4H, Ar-**H**), 7.35 (d, 2H, -C**H**=CH), 7.11 (d, 2H, -CH=C**H**) and (s, 2H, Ar-**H**), 6.94- 6.92 (d, 4H, Ar-**H**), 4.14-4.12 (d, 2H, C**H$_2$**OH), 3.96 (d, 2H, Ar-C**H**$_2$), 3.94 (d, 4H, OC**H**$_2$), 1.84-1.79 (m, 2H, C**H**) , 1.58-1.34 (m, 16H, aliphatic protons), and 1.01-1.91 (m, 12 H, C**H**$_3$). ^{13}C NMR ($CDCl_3$, 100

MHz) δppm: 151.11, 131.45, 127.75, 126..79, 121.80, 114.84, 110.19, 71.86, 69.31, 61.60, 39.86, 31.02, 29.34, 24.34, 23.19, 14.21, 11.41. FTIR (cm^{-1}): 3430, 2924, 2860, 1686, 1451, 1290, 1168, 1075. MALDI-TOF-MS: m/z calculated for $C_{32}H_{60}O_8P_2$: 658.92 and found 658.55 [M^+].

Synthesis of Dimethyl 2-((tert-butoxycarbonyl) L-aspartate (5): L-Aspartic acid (20.0 g, 0.15 mol) was dispersed in dry methanol (200.0 mL) and thionyl chloride (27.0 mL, 0.36 mol) was added drop-wise maintaining ice cold conditions under nitrogen atmosphere. After addition of thionyl chloride, the solution was brought to room temperature and refluxed at 60 °C for 6 h. After completion of esterification, the excess methanol and thionyl chloride were distilled off completely to get dimethyl-ester amine salt white mass, which was dissolved in 10 % Na_2CO_3 in water (320.0 mL). THF (320.0 mL) was added and the temperature of the reaction was maintained as 4 °C. BOC anhydride (34.0 mL, 0.15 mol) was added and after 30 minutes, the temperature of the reaction mixture was brought to 25 °C and stirred for 24 h. THF was distilled off completely and product was extracted in ethyl acetate and the organic layer was dried over anhyd. Na_2SO_4. The solvent was removed to get white solid which was purified by passing through silica column using ethyl acetate-pet ether system (1:6 v/v). Yield = 34.0 g (87 %). ^{1}H-NMR (400 MHz , $CdCl_3$) δ ppm: 5.48 (s, 1H, NH), 4.57 (s, 1H, -C**H**), 3.76 (s, 3H, -NHCOOC**H**$_3$), 3.70 (s, 3H, COOC**H**$_3$), 3.02-2.98 (dd, 1H, C**H**$_2$), 2.84-2.81 (dd, 1H, C**H**$_2$) and 1.45 (s, 9H, NHCOO(C**H**$_3$)$_3$). ^{13}C-NMR (100 MHz, $CDCl_3$) δ ppm: 171.61, 155.44, 80.24, 52.79, 52.08, 49.98, 36.73 and 28.35. MALDI-TOF-MS: m/z calculated for $C_{11}H_{19}NO_6$: 261.12 and found 284.09 [$M^+ + Na^+$] and 300.07 [$M^+ + K^+$].

Synthesis of Fluorescent Tagged L-Aspartic Polyester (P-OPV-x): Monomer **5** (0.50 g, 1.94 mmol), dodecanediol (0.20 g, 0.98 mmol) and triethylene glycol (0.13 g, 0.87 mmol) and hydroxyl functionalised OPV (64.0 mg, 0.097 mmol, 5 %) were weighed and taken in a melt condensation polymerisation test tube and melted at 100 °C and were purged with nitrogen gas. Ti $(OBu)_4$ (0.08 g, 2.3 mol %) was used as catalyst for melt condensation and was added to the melt which was further subjected to evacuation under vacuum of 0.01 mbar, and purged with nitrogen to remove traces of moisture from the melt content. This procedure was repeated thrice before raising the temperature of the melt reactor to 120 °C. The first step of polymerisation involved 4h purging with nitrogen followed by application of vacuum (0.02 mbar) for 2 h. The completion of polymerization was marked by formation of bright

yellow viscous solid. The polymer was purified by dissolving in minimum amount of THF followed by precipitation in cold methanol. Yield: 0.73 g (92 %). ^{1}H-NMR (400 MHz , $CdCl_3$) δ ppm: 7.47 (d, 0.19H, Ar-**H**), 7.38-7.34 (d, 0.09H, C**H**=C**H**),7.11 (d, 0.14 H, -C**H**=C**H**), 7.06 (d, 0.05H, -C**H**=C**H**), 6.90 (d, 0.20H, -Ar-**H**), 5.56 (m, 1H, -N**H**), 4.55 (s,1H, -C**H**), 4.32-4.25 (d, 0.94H, new TEG esters proton), 4.19 (s, 0.28H, new OPV ester protons), 4.15-4.04 (m, 2.48 H, -C$\mathbf{H}_2$OH and new aliphatic ester), 3.95 (d, 0.23H, -OC$\mathbf{H}_2$), 3.76-3.62 (m, 3H, -OC$\mathbf{H}_2$C$\mathbf{H}_2$), 3.06-2.78 (m, 2H, -C$\mathbf{H}_2$), 1.65 (m, 5H, aliphatic protons), 1.45 (s, 9H, BOC protons), 1.27 (m, 11H, aliphatic protons), 0.97-0.92 (m, 0.72H, -C$\mathbf{H}_3$).^{13}C-NMR (100 MHz, $CDCl_3$) δ ppm: 174.57, 171.10, 80.08, 70.62, 65.96, 65.26, 50.10, 46.65, 36.89, 29.60, 28.38, 25.94. A similar procedure was followed to synthesise P-OPV-12 using 10% OPV in feed and the details are given in supplementary data.

Synthesis of Non-Fluorescent Copolyester (P-0): The non-fluorescent copolymer was obtained using 50:50 mol ratio of triethylene glycol and 1,12 dodecandiol with respect to L-aspartic acid functional monomer. Monomer 1 (0.60g, 0.002 mol) and 1,12-dodecanediol (0.25 g, 0.001 mol), triethylene glycol (0.17 g, 0.001 mol) and titanium tetrabutoxide (0.005g, 1.47 mmol %) were used to synthesise the melt polymer as mentioned for the P-OPV-x polymer. Yield: 0.8 g (90 %). ^{1}H-NMR (400MHz, $CDCl_3$) ppm: 5.50 (bs, 1H, -N**H**), 4.56 (bs, 1H, -C**H**), 4.30–4.25 (m, 1.4H,COO-C$\mathbf{H}_2$$CH_2$O), 4.16–4.06 (m, 2.4H-, COO-C$\mathbf{H}_2$$CH_2$$CH_2$-), 3.77–3.61 (m, 3.9H, –C$\mathbf{H}_2$C$\mathbf{H}_2$O), 3.02–2.78 (m, 2H, NH-C$\mathbf{H}_2$), 1.63 and 1.27 (aliphatic protons) and 1.44 (s, 9H, BOC protons).^{13}C-NMR (100 MHz, $CDCl_3$) ppm: 171.10, 155.52, 80.09,70.62, 69.01, 65.96, 64.73, 64.02, 50.09, 36.90, 29.65, 28.38, 28.57.

Self Assemblies of Fluorescent P-OPV-x and P-0 copolymer: To study the self assembly of the fluorescent P-OPVs and P-0 copolymers in organic solvents , 0.1mg/mL polymer were dissolved in THF and drop casted on silica wafers, dried and subsequently spin coated with gold and observed using FESEM. The polymers with same concentrations were also dropcasted on mica sheets for their analysis using AFM technique. For aqueous self assembly, 5.0 mg of polymers were dissolved in 2.0 mL HPLC DMSO. To this was added Milli Q water (2.0 mL) dropwise. This solution was further dialysed against Milli Q water for 48 h by suspending the solution in a 3.5 kD semi-permeable membrane dialysis tube Spectrochem. The resultant dispersed solution of the polymers were filtered and lyophilized for further analyses.

Encapsulation of Dye: P-0 (5.0 mg) was dissolved in HPLC DMSO (2.0 mL) and Nile Red (0.1 mg dissolved in 2.0 mL HPLC DMSO) was added dropwise to it. Milli Q water (1.0 mL) was dropwise added with constant stirring. The stirring was carried on for 12 h and the solution thus obtained was subjected to dialysis. The reservoir water was continuously replaced to ensure complete removal of DMSO. After 48 h the solution was filtered and used for further analyses. Identical procedure was followed for loading NR to other polymers. Dye loading content (DLC) and Dye loading efficiency (DLE) were calculated using the following mathematical formulations by measuring the absorbance of fluorophore in the resultant dialysed solutions.[61]

DLC = [(weight of fluorophore encapsulated per mg polymer)/ weight of fluorophore loaded polymer] × 100.

DLE = [(weight of fluorophore loaded by the polymer/ total fluorophore used as feed)] × 100.

Photophysics and FRET experiments: The absorption and fluorescence studies were carried out keeping the optical density of OPV core as 0.1. OPV chromophore was excited at 397 nm and Nile Red chromophore was excited at 540 nm for obtaining emission spectra. For TCSPC life time studies nano-LED source with wavelength 371 nm and 550 nm for exciting OPV and Nile Red chromophores respectively were used, and their life time decay were obtained at emission maxima of 500 nm and 600 nm respectively. These decays were fitted by using DAS6 software. To determine molar extinction coefficient, various concentrations of OPV chromophore in THF where prepared ranging from 1.0 to 6.0 × 10^{-6} M and their absorbance were measured from UV spectrophotometer. The concentration of OPV chromophore was plotted against absorbance to determine the molar extinction coefficient as 78,000 M^{-1} cm^{-1}. The quantum yield of OPV chromophore was determined in water (dialyzed sample) and THF using quinine sulphate as reference (ϕ= 0.546 for quinine sulphate) following our reported procedure.[62]

Cytotoxicity studies: MTT assay, which is based on the metabolic activity of tetrazolium bromide, 3-4, 5 dimethylthiazol-2,5-phenyltetrazolium bromide in living cells, was employed for analysing the biocompatibility of the newly synthesised polyesters in cervical cancer (HeLa) cell lines, breast cancer (MCF 7) cell lines and wild type mouse embryonic fibroblast (WT-MEF) cell lines. Cells were cultured for a period of 16 h, in 96-well plates bearing 1000 cells in each well in 100 µl of DMEM along with 10% FBS solution. The media was further aspirated and the resultant cells were exposed to various concentrations of P-0 and P-OPV-6 polymers in triplicates. For the relative measure of the viable cells a blank control of cells

without any polymer was also maintained in triplicates. The cells were allowed to grow in the presence of the polymer for 72 h, and there after the media in each well was replaced with 100 µl of freshly prepared stock solution of MTT (containing 5 mg/mL MTT in PBS diluted to 50 µg/mL in DMEM). The MTT treated cells were allowed to incubate for 4h at 37 °C. The DMEM was further replaced with 100 µl of DMSO, which dissolved the purple formazan crystals obtained due to treatment of living cells to MTT. The 96-well plate was shook well before measuring the absorbance of the formazan crystals at 570 nm using Varioskan FLASH instrument. The mean of all the triplicate values were calculated (omitting any values deviating significantly from other two values), and the corresponding value of the blank cells were treated as 100 % figure and the cell viability caused by the polymers were calculated relative to the blank reading. The P-0 loaded with Nile Red was analysed for their cytotoxicity to MCF 7 cells using the same procedure as above. The similar procedure was also followed for the fluorescent tagged P-OPV-6 copolymer both in nascent and NR loaded form.

Confocal Imaging: A 6-well cell culture plate was loaded with glass cover-slips and MCF 7 cells were cultured in them in the presence of DMEM with 10% FBS, at a density of 1×10^5 cells each. The cells were incubated for 16 h prior to the experiments and were further treated with P-0 loaded with Nile Red, and P-OPV loaded with Nile Red, keeping the concentration of the respective fluorophores as 2µg/mL. After incubating for 4 h, the fluorophore containing media was aspirated and the cells were further processed for fixing. In a typical cell fixing experiment, the cells were washed twice with PBS (2 × 1.0 mL). The cells were fixed on the coverslips by incubating them for 10 min in the presence of 4 % paraformaldehyde (1.0 mL) at room temperature. For the P-0 loaded nanoparticles treated cells, the cells were stained with DAPI while incubating for 2 min in dark. However for the P-OPV-6 loaded nanoparticles treated cells, the cells were stained with phalloidin by incubating them with phalloidin green for 20 min. The cells were rinsed once with PBS, and the coverslips were mounted on fresh glass slides using Fluoromount mounting medium. The coverslips were dried overnight in dark. The cells thereby fixed on the glass slides were then imaged using confocal microscope using the lasers 405 nm (as blue channel), 561 nm laser (for red channel) and laser 488 nm (for green channel). The images thus obtained were processed in Image J software. For FRET experiments the cells were not stained with DAPI and phalloidin to avoid any interference with OPV and NR emission.

Lysosomal Tracking of polymer nanoparticles: In a typical experiment, 25000 cells were seeded in each well of an 8-well live cell chamber, and incubated at 37°C to grow for 16h. P-OPV+NR, P-0+NR and P-OPV were administered to the cells after replacing with fresh media. The concentration of chromophores were maintained same as that of confocal imaging experiments. Cells were incubated with the nanoparticles further for 4h, and the media was removed from the cells. The cells were rinsed with PBS once, and 50.0 nM Lyso tracker® Green DND-26 was added to them and were immediately imaged under CSLM confocal microscope. Lyso tracker was excited using Laser source of 488nm and the images obtained were processed using Image J software.

FACS analysis: The quantification of the fluorophore taken up by cells was successfully carried out using flow cytometry cell analyzer. HeLa cells were seeded at a density of 1×10^5 in each well of a 6 well plate and were incubated and allowed to grow for 16 h under the presence of DMEM with 10% FBS at 37 °C. P-0 loaded with Nile Red and the corresponding free Nile Red (2.0 μg) were exposed to the cells, which were further incubated for 4 h. The media was aspirated from each well and the treated cells were washed with PBS (1.0 mL), and further, the cells were trypsinised by treating with trypsin for 1 min at 37 °C. Cells were centrifuged and pelleted down and re-suspended in 1.0 mL PBS. The suspension of cells was analysed using BD LSRFortessa SORP cell analyzer with 5 lasers and 18 colour detectors. The 561 nm laser was used to excite Nile Red and the bandpass filter was maintained at 610 ± 10 nm. A population of 10,000 cells were screened for emission histograms.

Results and Discussion

Synthesis of Fluorescent-Tagged OPV Polymers

Oligo-phenylenevinylene (HO-OPV-OH) was chosen as π-conjugated fluorophore diol and it was synthesized by multi-step organic reactions starting from hydroquinone as shown in scheme-1. Hydroquinone was converted into bis(2-ethylhexyloxy) benzene (**1**) using 2-ethyl-hexyl bromide and it was bromomethylated to yield compound (**2**). Compound **2** was reacted with $P(OEt)_3$ to yield bis-phosphonate ester (3). 2-Bromoethanol was coupled with 4-hydroxy benzaldehyde to yield compound **4**. The bis-phosphonate ester (**3**) was subjected to Witting-Horner reaction with **4** in the presence of base to yield the HO-OPV-OH following our earlier procedure.[33] L-Aspartic acid was converted into melt polymerizable multi-functional monomer (**5**) as shown in scheme 1.[55] Two carboxylic acid functional groups were converted into methyl esters and the amine was protected by BOC group. The monomer (**5**) was polymerized with HO-OPV-OH, triethylene glycol (TEG) and dodecanediol (DD) to yield new classes of fluorescent-tagged amphiphilic polyesters (P-OPV-x) (see scheme-1).

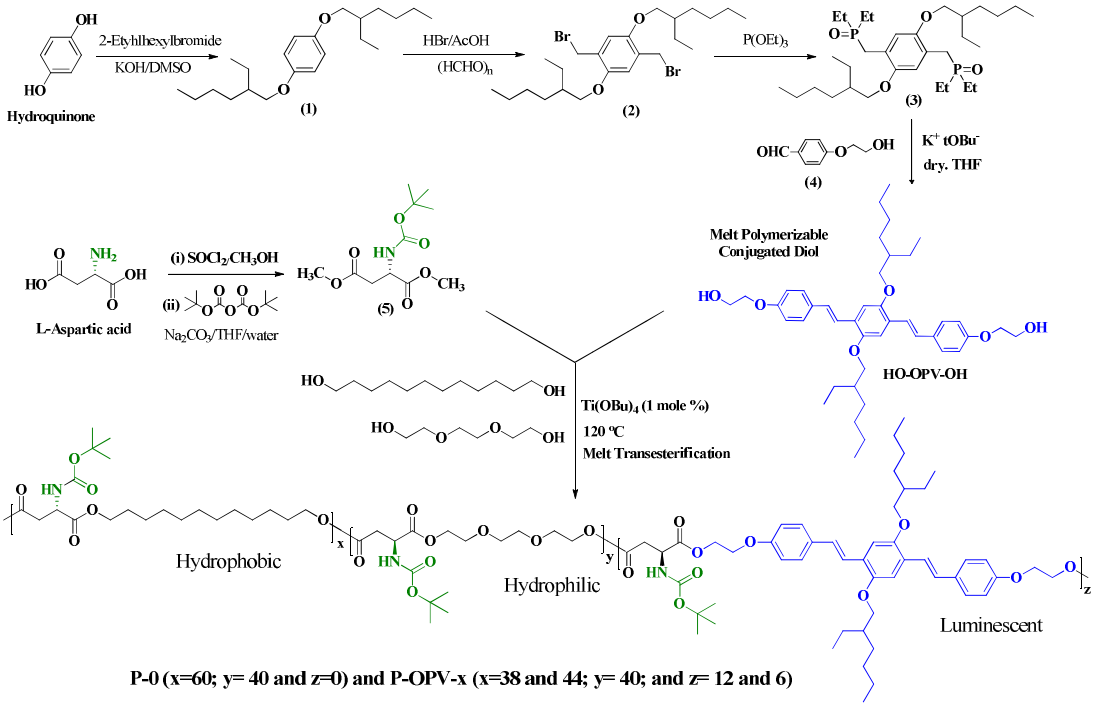

Scheme 1. *Synthesis of fluorescent OPV-tagged L-aspartic acid amphiphilic polyester.*

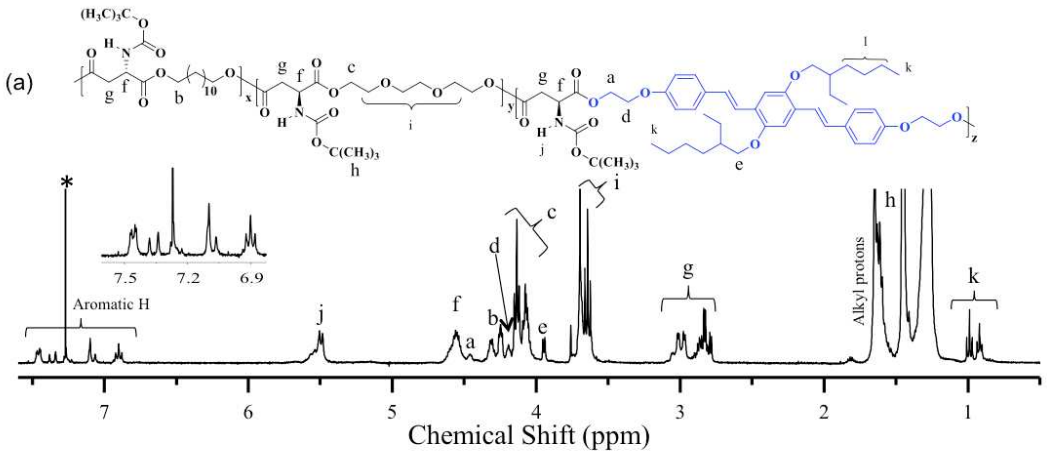

(b) Table containing the composition of polymers, molecular weights, and thermal properties

Polymer	DD unit[a] (^{1}H-NMR) [a]	TEG unit (^{1}H-NMR) [a]	OPV unit (^{1}H-NMR) [a]	M_n (g/mol) [b]	M_w (g/mol) [b]	M_w/M_n	T_g (°C) [c]	T_D (°C) [d]
P-0	60.0	40.0	0	7000	16000	2.6	-13.83	207
P-OPV-6	54.0	40.0	6.0	8100	18000	1.9	-9.83	190
P-OPV-12[e]	44.5	43.5	12.0	4100	8200	2.0	-7.76	200

[a] Determined by ^{1}H-NMR in $CDCl_3$. [b] Determined by GPC in THF at 25°C. [c] Determined by DSC at 10°C/min in heating cycle. [d] Determined for 5 % weight loss by TGA at 10°C/min under N_2. [e] The polymer was partially soluble in THF

Figure 2. *(a) ^{1}H-NMR spectrum of P-OPV-6 in $CDCl_3$. (b) Table contains the composition of polymers, their molecular weights and thermal properties.*

The polymerization was carried out at 120 °C using $Ti(OBu)_4$ (~1 mole %) as catalyst under solvent free melt conditions. In this process, the di-ester underwent transesterification reaction to yield polyesters, and during this melt process the BOC urethane was found to be completely inert.[51,55] For all the polymerization reactions; the TEG content was always retained as 50 mole % in the feed in order to maintain the required hydrophilicity in the polymer backbone. The amounts of DD (40 and 45 %) and HO-OPV-OH (10 and 5 %) were varied in the feed so that the total diols content (TEG + DD + HO-OPV-OH) was always retained as 100 % in the feed (diols to monomer **1** ratio was maintained as 100: 100). The chemical structures of the OPV-tagged fluorescent polymers were confirmed by ^{1}H NMR and the spectrum for polymer is given in figure 2a (see more spectra for other polymers in the supporting information). The peaks in the spectrum were assigned to different types of protons in the chemical structure by alphabets. The spectrum showed newly formed ester peaks OPV–C**H**$_2$-OOC (proton-a) at 4.45 ppm, TEG-C**H**$_2$-OOC (proton-b) at 4.31 ppm, and DD-C**H**$_2$-OOC 4.15 ppm (proton-c), respectively. Further, the spectrum also showed peaks for the protons OPV–C**H**$_2$CH$_2$-OOC (proton-d), Ar-OC**H**$_2$-CH-EH (proton-e) and aromatic-**H**

at 4.22 ppm, 3.95 ppm and 6.80- 7.50 ppm, respectively. All other protons were assigned with respect to their chemical structure. The comparison of the peak intensities of protons a, b and c gave the actual incorporation of OPV, TEG and DD amount in the amphiphilic polymer backbone (see table in figure 2). The intensities of BOC urethane protons at 1.44 ppm (proton-h) remained constant and it was not disturbed by the melt transesterification process.[54] This confirmed the selective transesterification of diesters towards diols in the formation of expected amphiphilic polyester structure. These amphiphilic polymers are referred as P-OPV-x, where x = 6 and 12 with respect to the actual incorporation of OPV amount in the polymer. The polymer without OPV chromophore is referred as P-0. The molecular weights of the polymers were determined by gel permeation chromotograpy and the details are given in the table in Figure 2b. All the polymers showed mono-modal distribution (see SF-1) and they exhibited M_n = 7.0- 8.0 × 10^3 g/mol and M_w= 16.0- 18.0 × 10^3 g/mol with polydispersity of ~ 1.9 to 2.6 (polydispersity of ~2.0 is typically expected for condensation polymerization). The sample P-OPV-12 was found to be partially soluble in THF for GPC analysis. The polydispersity of the polymers are little higher than 2.0 which is typically acceptable for the melt polycondensation approach.[51] The degree of polymerization ($X_n = M_n/M_o$) or average number of repeating units were determined as 22- 25 which suggested the formation of moderate to high molecular weight polymers for lab-scale melt polymerization process.[50] The dn/dc value for the polymer P-OPV-6 was determined by GPC chromatograms using various polymer concentrations (see SF-2). The dn/dc value was determined as 0.01 for P-OPV-6 which is similar to that of dn/dc value reported for aliphatic random copolymer poly(butyleneterephthalate)-poly(butylene adipate).[63] Thermogravimetric analysis showed that the polymers were stable up to 280 °C (see SF-3) and the differential scanning calorimetry exhibited only glass transition temperature in the range of -5 to 30 °C with respect to the amorphous nature of the polymers (see SF-4).

Aromatic π-stack Driven Polymer Self-assembly

π-Conjugated chromophores are very well known to undergo strong aromatic π-stacking due to the overlap of π-cores depending on the solvents in which they are dissolved or dispersed.[57] Typically the polymer chains adopt expanded chain conformation and are largely isolated in dilute concentration in good solvents. In poor solvents or in the mixtures of good+poor solvents, the polymer chain-chain interactions become predominant which lead to the formation of micron-sized polymer aggregates.[59] In the present case, the L-aspartic acid polymer system was designed with π-conjugated OPV chromophore; thus, the polymer

chains are expected to experience strong aromatic π-π stacking interactions (see schematic in Figure 3a). Since the polymer was designed with hydrophilic TEG-units, hydrophobic DD-units and aromatic OPV chromophores; they were expected to experience both amphiphilic and aromatic π-stacking non-covalent interaction together. To study these interactions, the polymer samples were subjected to photophysical studies in good solvent (tetrahydrofuran, THF), dialyzed aqueous solutions and in thin film. The absorbance spectra of P-OPV-6 in aqueous solution, thin film and in THF are showed in figure 3b (see SF-5 for P-OPV-12). The molar extinction coefficient of OPV was determined as 78,000 $M^{-1}cm^{-1}$ in THF (see SF-6).The dialysed polymer solution and thin film spectra showed 10 nm red-shift compared to polymers in THF. Additionally, a hump was observed with respect to aggregates of OPV chromophores at 475 nm. This trend suggested that the OPV chromophores were completely isolated and they were not aggregated in THF (good solvent). On the other hand, the inter-chain interactions became predominant and the OPV chromophores underwent strong aromatic π-stacking interactions in the aqueous medium. The extent of OPV aromatic π-stacking seem to have reached a maxima (10 nm red-shift) in the aqueous medium which is almost similar to that in thin film.

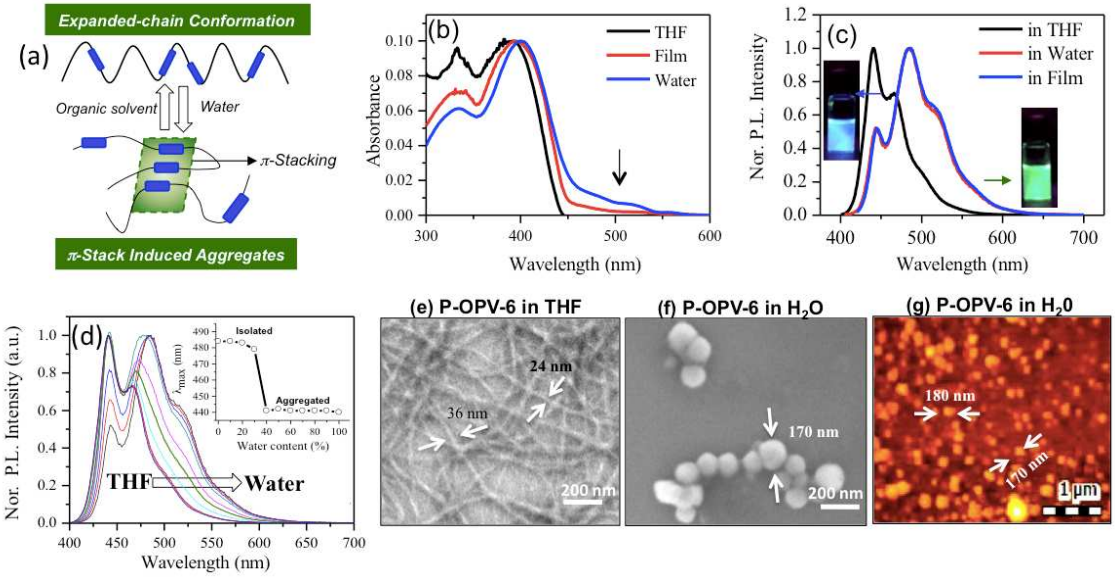

Figure 3. *(a) Schematic representation of aromatic π-π stacking in P-OPV-x polymers with respect to the good (THF) and poor (water) solvents. Absorbance (b) and emission (c) spectra of P-OPV-6 in THF, dialyzed aqueous solution and thin film (λ_{ex} = 397 nm and O.D. = 0.1). The photographs of the vials indicate the emission from polymer in THF and water. (d) Emission spectra of P-OPV-6 polymer in THF/water solvent combinations. The in-set figure showed the plot of emission maxima with respect to solvent compositions. FESEM images of P-OPV-6 in THF (e) and in water (f). AFM images of P-OPV-6 in water (g).*

Emission spectra of the OPV chromophores (see figure 3c) were found to be more sensitive to the aromatic π-stacking phenomena. OPV polymers showed the characteristic emission maxima at 440 nm with respect to isolated chromophores in THF.[57] The peak was red-shifted by 60 nm in aqueous sample (also in thin film) which was attributed to the OPV aggregates. The photographs of polymer vials showed blue-luminescence in THF and greenish blue luminescence in water with respect to their isolated and aggregated chromophores (see Figure 3c). The extent of the peak shift was found to be same in P-OPV-6 and P-OPV-12 (see SF-7) suggesting that minimum 6 % OPV chromophore incorporation in the L-aspartic acid amphiphilic backbone was sufficient enough to attain maximum aggregation characteristics. The quantum yield of P-OPV-6 was determined as ϕ =0.30 and 0.74 for dialyzed aqueous sample and in THF, respectively (using quinine sulphate as reference, see SF-8 for detail calculation). The quantum yields of the polymer samples were very good and they were matching with the reported values for OPV chromophores.[57-58] The dialyzed sample of P-OPV-12 was also found to be turbid and relatively less soluble which indicates that higher amount of OPV incorporation decreases the polymer water solubility. Thus, for all further analyses only the sample P-OPV-6 was used in the present investigation. To study the effect of solvent environment on the aromatic π-stacking interactions, the P-OPV-6 sample was subjected to photophysical studies in THF+water solvent combinations (see Figure 3d). With increase in the water content in the solvent mixture, the emission peak was shifted towards longer wavelength region (see absorption spectrum in SF-9). The extent of π-aggregation in water+THF composition was further quantified by plotting their λ_{max} and the plot in figure 3d in-set showed a break point at 40 % water in solvent mixture. It clearly suggested that the isolated OPV amphiphilic polymer chains underwent aromatic π-stacking upon increasing the water content in the solvent mixture. To visualize the polymer aggregates, the samples were subjected to field emission scanning electron microscope (FESEM) and atomic force microscope (AFM) analysis. The P-OPV-6 in THF showed (see Figure 3e) thin helical nano-fibers having width 35 ± 8 nm. The length of these nano-fibres was measured to be ~ 2.0 μm which indicated their high aspect ratio ~ 40 to 60 with respect to long-range supramolecular assemblies. The water dialyzed P-OPV-6 sample (see Figures 3f and 3g) showed exclusively the formation of spherical nanoparticles of < 200 nm in size. Both FESEM and AFM analysis have provided direct evidence for the morphological transformation from nano-fibrils to stable nanoparticles upon varying the solvent micro-

environments from THF to water. Based on the photophysical studies, FESEM and AFM morphology, it may be concluded that the polymer chains adopt expanded chain conformation to produce helical nano-fiber morphology in good solvent like THF whereas they produced stable spherical nanoparticle in aqueous medium. In the present case, the aqueous nanoparticles were stabilized through both OPV aromatic π-stacking and hydrophilic interactions.

Encapsulation Capabilities and Cellular uptake

The encapsulation capabilities were studied for both luminescent amphiphilic polyesters with OPV chromophores (P-OPV-6) and non-luminescent polyester P-0 (polymer without OPV). The polymers were loaded with water insoluble commercial fluorescent dyes such as Nile red (NR), Rose Bengal, Fluorescein and Congo red by dialysis method. Among all the fluorophores, only NR was found to be loading in significant quantity both in P-OPV-6 and P-0 nanoparticles. NR has good absorbance (molar extinction coefficient = 38,000 M^{-1} cm^{-1})[64] and reasonably good quantum yield (ϕ = 0.018,);[65] hence, it is suitable as fluorophore for bioimaging applications. The dye loading content (DLC) was found to be 5.0 % and 4.0 % in P-OPV-6 and P-0 nanoparticles, respectively (DLEs were obtained as 50 % and 40 %, respectively). The NR loaded nanoparticles were referred to as P-OPV-6+NR and P-0+NR. DLS histograms of NR loaded P-0 showed the size of the nanoparticles as 140 ±2 nm (shown in figure 4a). The absorption and emission properties of NR fluorophore were retained even after loading and these characteristics are summarized in SF-10. The DLS histograms of aqueous samples of P-OPV-6 and P-OPV-6+NR showed the existence of < 200 nm size nanoparticles (see Figures 4b and 4c).

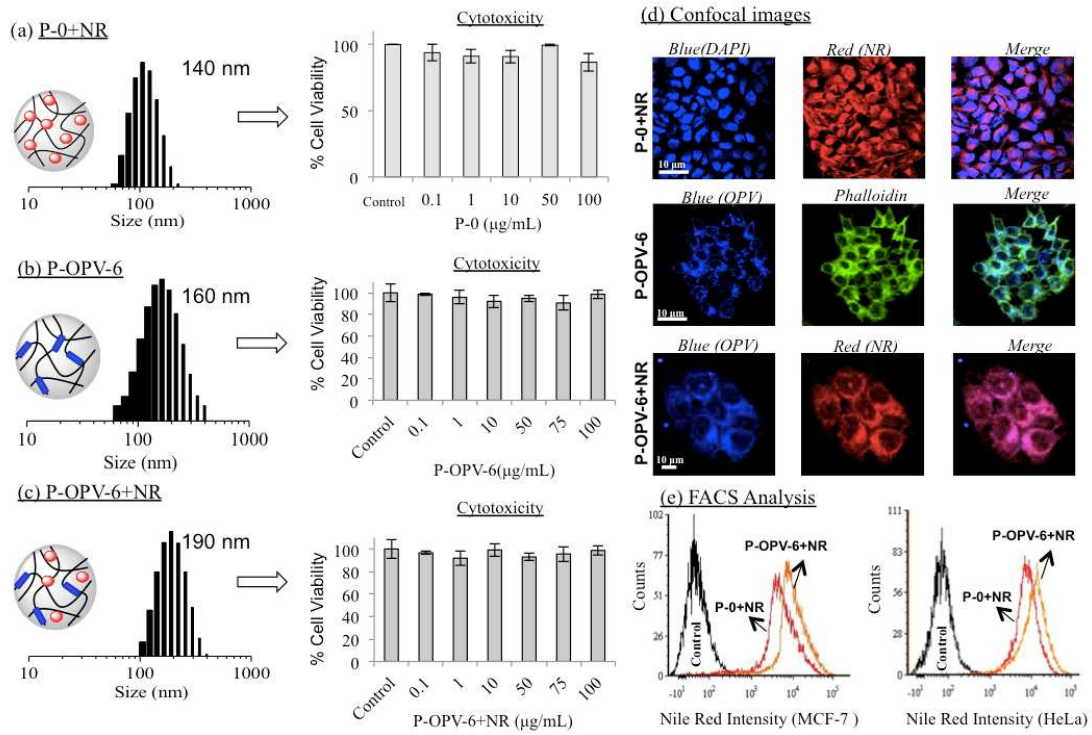

Figure 4. *DLS histograms and cytotoxicity in MCF7 cell lines for P-0+NR nanoparticles (a), P-OPV-6 nanoparticles (b), and P-OPV-6+NR nanoparticles (c). Confocal microscope images of P-0+NR, P-OPV-6 and P-OPV-6+NR nanoparticles(d). FACS analysis histograms of P-OPV-6+NR in MCF7 cell lines and HeLa cell lines (e) (10000 counts are used)Cells were incubated for 4h.*

Cytotoxicity of the nanoparticles P-OPV-6, P-0+NR and P-OPV-6+NR were studied in breast cancer (MCF 7), cervical cancer (HeLa) and normal (wild-type MEF) cell lines. The cytotoxicity of nanoparticles in MCF 7 cells are given in Figure 4, and data for HeLa and WT-MEF cell lines are given in SF-11. The polymer nanoparticles P-OPV-6, P-0+NR, P-OPV-6+NR were found to be non-toxic to cells up to 100 μg/mL. The biocompatibility exhibited by these polymer nanoparticles is one of the desirable traits for biomedical applications. To investigate the cellular uptake, P-0+NR, P-OPV-6 and P-OPV-6+NR nanoparticles were internalised in MCF 7 cells and subjected to CSLM microscope analysis. Confocal images were visualized at blue ($\lambda_{excitation}$ at 405 nm laser) and red ($\lambda_{excitation}$ at 561 nm laser) channels and their confocal images are shown in Figure 4d. Top most row corresponding to P-0+NR showed DAPI stained nucleus of cells and the emission from NR was largely observed in the cytoplasm in the cells. The merged image of NR and DAPI showed no overlap of their red and blue emission at the nucleus indicating the accumulation of P-0+NR largely in the cytoplasm and not at the nucleus. The second row in the figure 4d

shows the uptake of P-OPV-6 blue luminescent nanoparticles. The actin filament skeleton of the cells were stained with green emitting phalloidin (the nucleus is not stained; thus it appears dark) and the blue emission from OPV chromophores in the polymer was clearly observed. This was further supported by the merged image. The cellular uptake of P-OPV-6+NR showed dual emission with respect to OPV and NR in the blue and red channels, respectively (not stained with DAPI). The merged image showed distinct magenta colour from the cytoplasm arising by the combination of emission from OPV plus NR. These studies confirmed the ability of the polymer nanoparticle to carry fluorophores and internalise them in the cytoplasm in the cells. Further, fluorescence activated cell sorting (FACS) was used to substantiate the confocal microscopy results of internalisation of the biomarkers. To quantify the cellular uptake of the nanoparticles, flow cytometry experiments were carried out for P-0+NR and P-OPV-6+NR both in MCF 7 and HeLa cell lines (see figures 4e). The intensities of NR delivered in HeLa cells and MCF 7 cells were relatively high and almost comparable. The high luminescent intensity for NR in FACS analysis is in very good agreement with the confocal images and it validated the ability of newly designed amphiphilic polymer nanoparticles taken up by the cancer cells. Thus, the newly designed OPV conjugated L-aspartic polymer nanoparticles were stable in aqueous medium and retained the luminescent characteristics and readily transported across cell membranes into the cytoplasm of cancer cells.

FRET Probe Based on NR and OPV polymer

Fluorescence resonance energy transfer (FRET) from donor-acceptor fluorophores are excellent yet challenging probe for cellular imaging in cancer treatment. Having tested the OPV tagged L-aspartic polymer nano-scaffold for loading NR; here efforts were taken to construct the new FRET probe between OPV donor and NR acceptor for bio-imaging. The possibility of FRET occurrence was assessed by the FRET overlap integral between the emission spectrum of donor (OPV in the present case) and absorbance spectrum of acceptor (NR). The overlap of these spectra is shown in figure 5a and it was estimated to be more than 75 % for the occurrence of efficient FRET process. Figure 5b shows a schematic energy diagram of FRET between OPV donor and Nile Red acceptor. Upon selective photoexcitation (λ_{ex} = 397 nm); the OPV excitation energy can be utilized for two processes: (i) radiative self blue-emission of OPV chromophores at 450-525 nm, and (ii) transfer of excitation energy from OPV to NR through FRET process thereby red-emission can be observed from NR at

600 nm. In the second process, the blue-emission from the OPV chromophore was expected to decrease or vanish due to the excitation energy transfer to NR.

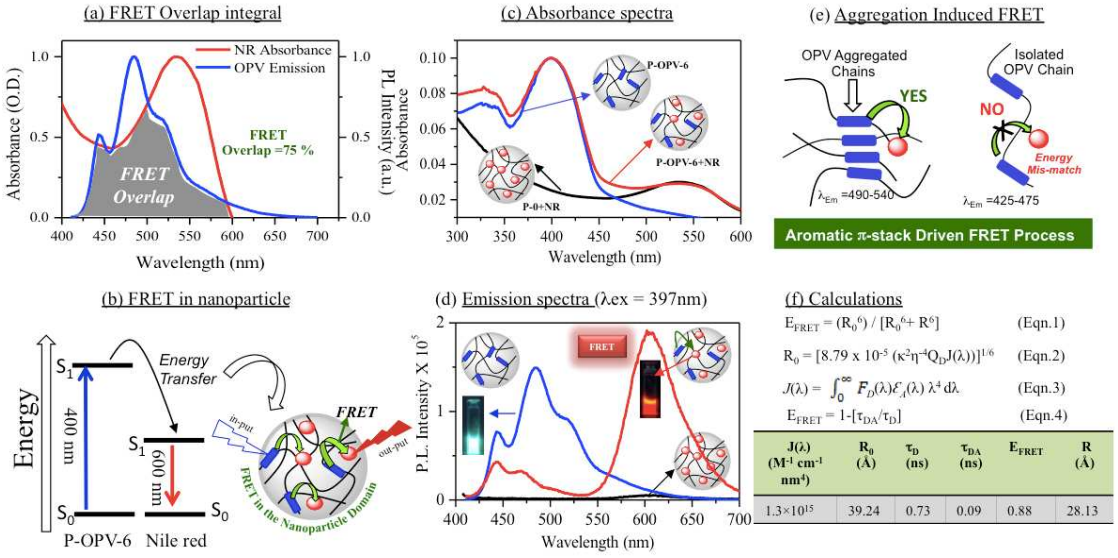

Figure 5. *(a) Overlap integral between the emission spectra of P-OPV-6 and absorbance spectra of NR. (b) Energy diagrams for the FRET process. (c) Absorbance spectra of P-0+NR, P-OPV-6 and P-OPV-6+NR in aqueous medium. (d) Emission spectra of P-0+NR, P-OPV-6 and P-OPV-6+NR [λ_{ex} = 397 nm in aqueous medium]. (e) Schematic representation of OPV aggregates on the occurrence of FRET process in polymer nanoparticle domain. (f) Equations used for calculation FRET in P-OPV-6+NR.*

The absorbance spectra of aqueous nanoparticles of P-OPV-6, P-OPV-6+ NR and P-0+NR are shown in figure 5c. The concentrations of OPV species in P-OPV-6 and P-OPV-6+NR were maintained as 0.1 O.D. and NR was maintained as O.D. = 0.03. The absorption maxima corresponding to OPV was observed at 397 nm and NR showed characteristic absorbance at 540 nm (see figure 5c). The three nanoparticles were excited at 397 nm (with respect to OPV absorbance) and their emission spectra were recorded and shown in figure 5d. At 397 nm excitation, the P-OPV-6 samples showed emission maxima at 480-500 nm with respect to the emission from OPV aggregated chromophores. At this excitation wavelength (397 nm), the P-0+NR nanoparticles (without OPV chromophore) did not show emission peak neither in the OPV nor in the NR regions. This confirmed that the NR chromophores were not excited at the OPV excitation wavelength. At 540 nm excitation (with respect to NR); the samples P-0+NR and P-OPV-6+NR showed emission exclusively for NR emission (see SF-12). Interestingly at 397 nm excitation; the NR loaded OPV polymer nanoparticle (P-OPV-6+NR) exhibited high intense emission peak at 600 nm from NR chromophores (see Figure 5d). This observation was attributed to the excitation energy transfer from the OPV to

NR chromophores in the nanoparticle domain. In this experiment, the OPV self-emission also drastically decreased due to the partial excitation energy transfer to NR fluorophore. This residual OPV self-emission appeared at 450 nm with respect to isolated OPV chromophores (compare figure 5d with figure 3c). It suggests that the OPV chromophores existed both as isolated and aggregated states in the polymer nanoparticle; however, only the aggregated OPV chromophores were involved in the excitation energy transfer to NR. The isolated OPV chromophores which did not participate in the FRET event showed self-emission at 450 nm. A model for this OPV aggregated chromophore directed FRET process is depicted in figure 5e. A control experiment was carried out to prove the aggregated OPV chromophore directed FRET hypothesis in the polyester nanoparticle domain. In this experiment, THF was added into the dialyzed P-OPV-6+ NR nanoparticle and the emission spectra were recorded using 397 nm excitation (see SF-13). The addition of THF immediately destabilized the aggregation of OPV chromophores rendering them isolated in the solution (as evident from the figure 3d). As soon as THF was added, the FRET emission peak at 600 nm completely disappeared and the self-emission with respect to isolated OPV chromopheores appeared at 450 nm (see SF-13). This control experiment confirmed the hypothesis that FRET process exclusively occurred between aggregated OPV and NR as shown in Figure 5e. Förster distance between the donor-acceptor is an important criterion for occurrence of the efficient FRET process (see equations in Figure 5f). The FRET efficiency is represented by the equation: $E_{FRET} = (R_0^6) / [R_0^6 + R^6]$, where R and R_0 are the distance between donor and acceptor molecules and Förster distance at 50 % of FRET process.[6] E_{FRET} was obtained from the fluorescence life times of donor molecule alone (τ_D) and donor in the presence of acceptor (τ_{DA})[6] using the equation: $E_{FRET} = 1-[\tau_{DA}/\tau_D]$. The values were determined by detailed calculations and the method is described in the supporting information (see SF-14). TCSPC fluorescence decay profiles of OPV chromophores in nascent polymer P-OPV-6 and in the presence of FRET acceptor NR (in sample P-OPV-6+NR) were recorded (see SF-14). As expected the OPV fluorescent intensities decay much faster in the presence of NR.[6]The decay rate constants were determined and employed in the E_{FRET} equation. Based on these calculations, the Förster distance and donor-acceptor distance were obtained as 39.24 Å and 28.13 Å, respectively (see table in Figure 5f), which are much lower than the < 50 Å cut-off.[6] The FRET efficiency E_{FRET} was estimated to be 88 % and these parameters are clearly evident for the efficient FRET process between the OPV chromophore and encapsulated NR fluorophore within the L- aspartic polymer nanoparticle domain (see Figure 5e). Based on the above detail photophysical studies and energy calculations, it can be concluded that the newly

designed OPV tagged L-aspartic polymer nanoparticle provided appropriate nanoparticle geometry for efficient FRET probe based on OPV and NR donor-acceptor pair.

Enzymatic-biodegradation of FRET Probe

Aliphatic polyester linkages are susceptible for both hydrolytic degradation at the extracellular level and enzymatic-biodegradation by the lysosomal enzymes at the intracellular compartments.[66] Lysosomes are typically abundant with lipase, chymotrypsin, trypsin and esterase enzymes and they were employed for the biodegradation studies of poly(ester-amide)s,[39-40] polypeptides[67] and aliphatic polyesters[55, 68-69] by us and others. Recently Wang et al. reported that glutathione (GSH) was also capable of degrading poly(ester-amides) in the cytoplasm.[70] Based on this available literature, we have chosen four different enzymes: esterase, chymotrypsin, trypsin, papain[71] and GSH redox species to study the biodegrading ability of the L-aspartic polyester nanoparticles and their influence on their FRET process. Prior to this, the stability of the polymer nanoparticles were tested by incubating the P-OPV-6 (in the absence of enzymes) at 37 °C in PBS (pH = 7.4). The emission spectra were recorded at various time intervals and their spectra are shown in figure SF-15. The intensity of emission peak at 440 nm was unaltered indicating the high stability of the FRET nanoparticles under physiological conditions. In the presence of the enzymes, the aliphatic polyester backbone underwent cleavage and disrupted the nanoparticle structure. This led to the separation between OPV and NR and thus causing loss or turn-off of the FRET process (see figure 6a). This influence of enzymes on the FRET probe functioning was studied by monitoring the response of nascent P-OPV-6 and P-OPV-6+NR loaded nanoparticles in the presence of various lysosomal enzymes. The effect of esterase enzyme on the self-blue emission of nascent P-OPV-6 nanoparticles and FRET red-emission from P-OPV-6+NR nanoparticles are shown in figures 6b and 6c, respectively.

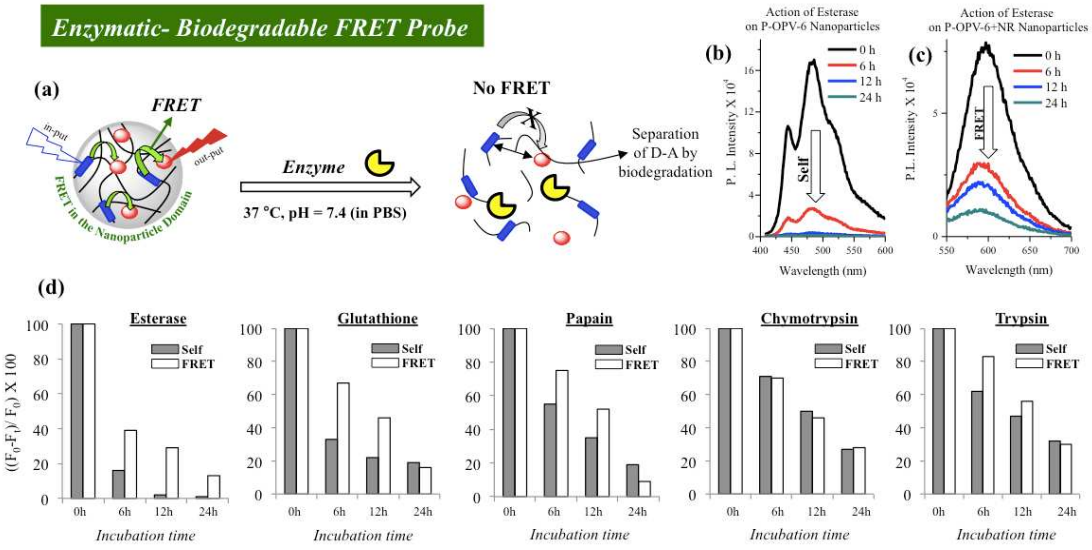

Figure 6. *(a) Schematic diagram of P-OPV-6+NR nanoparticle and the action of esterase enzyme on the biodegradation of the nanoparticle. (b)Emission spectra of P-OPV-6 nanoparticles in the presence of 10 U esterase enzyme at 37 °C (in PBS). (c) Emission spectra of P-OPV-6+NR nanoparticles in presence of 10U esterase enzyme at 37 °C (in PBS). (d) The plot of OPV self emission and FRET red-emission of P-OPV-6+NR in presence of enzymes in PBS (pH = 7.4) at 37 °C at various incubation times.*

The self-emission of OPV chromophore drastically reduces with increase in time with respect to the biodegradation of the polyester backbone by esterase enzyme. This process altered the hydrophilic and hydrophobic balance of the polymer and thereby causing the disruption of OPV self assemblies. A similar observation was made in the case other enzymes and GSH and these details are given in SF-16. The NR loaded P-OPV-6 nanoparticles (P-OPV-6+NR) exhibited drastic decrease in the NR emission and the FRET process was almost lost within 24 h of enzyme action (figure 6c). The change in the PL intensity was plotted using the expression: $[F_0\text{-}F_t]/F_0$ x100 where F_0 and F_t are emission intensity at initial and at time 't' with respect to the incubation time. These values were plotted against incubation time and shown in figure 6d. GSH and papain showed a reduction in emission intensity of both OPV self emission and FRET emission up to 20 % in 24 h. The reduction in self emission and FRET signal were up to 30 % in case of chymotrypsin and trypsin in 24 h (see figure 6d). Higher efficiency of reduction in the PL intensity was observed for esterase enzymes and within 12 h the polymer degraded completely. This observation revealed that all the enzymes employed in this experiment were capable of degrading the polymer chains; however the esterase enzyme was found to be more active than others. These studies confirmed the enzymatic-biodegradation nature of the polymer chains at intracellular

conditions. Further, the amphiphilic polyesters are stable at extracellular conditions and maintained their FRET characteristics. Up on being taken up by cells, the probes would slowly biodegrade by enzymes and it would lead to loss of both OPV self-emission and FRET emission in 6-8 h time. Since, most of the intracellular bio-imaging applications are done for < 12 h, thus, the probe has sufficient stability for the imaging at the intracellular level. Once the imaging job is done, the probe would undergo slow biodegradation at the cellular level which is desirable for their excretion from the point of target.

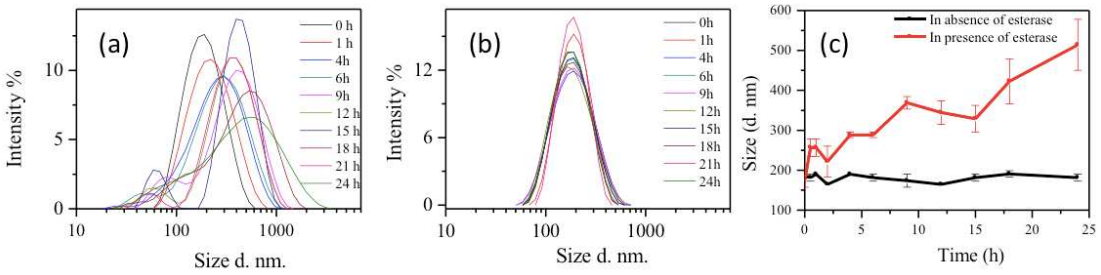

Figure 7. *(a) DLS histograms of P-OPV-6 in the presence of esterase enzyme in PBS (pH = 7.4) at 37 ℃. (b) DLS histograms of P-OPV-6 in PBS (pH = 7.4) at 37 ℃. (c) Plot of DLS size of the polymer nanoparticles in the presence and absence of esterase enzymes.*

The enzymatic-biodegradation of aliphatic polyester chains can be readily monitored by the DLS analysis. The amphiphilicity of the polyester nanoparticles is disturbed by the biodegradation process and the degraded oligomers thus have relatively poor solubility or dispersion in water. As a result, the oligomers tend to precipitate from the aqueous medium which significantly increases the particle sizes from nano- to submicron range.[56,68] To study the biodegradation of P-OPV-6, DLS experiment was carried out in PBS (pH = 7.4) at 37 ℃ in the absence or in the presence of esterase enzyme. Upon biodegradation the nanoparticles do not possess tightly packed self-assembly; as a result, the particle size distribution transformed from mono to multi-modal as shown in figure 7a. In the absence of the enzyme, the sizes of the P-OPV-6 nanoparticles did not show any appreciable change (see Figure 7b). This experiment confirmed that the P-OPV-6 nanoparticles were stable at extracellular conditions and exclusively underwent biodegradation in the presence of enzymes. The average sizes of the nanoparticles obtained from DLS were plotted against incubation time and are shown in figure 7c. The polymer nanoparticle was found to be stable up to 6-8 h and it gradually degraded up to 24 h in the presence of esterase enzyme. After 24 h incubation, the biodegraded polymer sample was lyophilized and subjected to MALDI-TOF MS and GPC analysis (see SF-17). The mass spectra showed peaks with respect to DD-Aspartic acid-

TEG, Aspartic acid-TEG, and OPV-Aspartic acid-TEG degraded oligomeric units confirming the occurrence of the enzymatic-degradation of the aliphatic polyester backbone. The GPC chromatograms of degraded sample showed the disappearance of the high molecular weight chains and appearance of peaks with respect to oligomers that come along with solvent. Based on the above studies, it can be summarized that the newly designed OPV-tagged L-aspartic polyester FRET probe is highly biodegradable by wide range of lysosomal-enzymes, non-toxic, biocompatible and also suitable for bio-imaging applications.

FRET Probe for Bio-imaging in Cancer cells

To demonstrate the FRET process at the intracellular level, two cancer cell lines-breast cancer (MCF 7) and cervical cancer (HeLa), and also normal wild-type MEF cell line were chosen. Confocal microscopy with selective photoexcitation for OPV chromophore was employed to observe the FRET phenomenon in P-OPV-6+NR nanoparticles. P-OPV-6 and P-0+NR nanoparticles were chosen as donor and acceptor controls, respectively. The cells were incubated at 37 °C for 4 h uptake. The cells administrated with P-OPV-6 and P-0+NR nanoparticles were excited with 405 nm and 561 nm lasers, respectively and the images were captured both at blue (410 – 460 nm) and red channel (570- 635) depending upon the requirement. These confocal images are shown in figure 8. At 405 nm excitation (OPV chromophores), the cells having P-OPV-6 nanoparticles showed bright blue-luminescence and the cells were clearly visible in the blue channel and no signal was observed in the red channel (see Figure 8a). At 561 nm excitation (NR chromophore), the P-0+NR administration in cells showed bright red-emission in red channel and no signal was observed in the blue channel (see Figure 8b). This confirmed that both OPV and NR chromophores retained their individual emission characteristics without cross-talking with each other upon photoexcitation in CSLM experiments. Interestingly at 405 nm excitation (OPV chrmophores), the P-OPV-6+NR nanoparticles exhibited blue-emission from OPV chromophore (in blue channel) and bright red-emission from NR (in red channel) followed by the occurrence of FRET between OPV donor and NR acceptor (see Figure 8c). The merged images showed magenta colour due to the combination of blue and red signals confirming the occurrences of FRET process at the intracellular level. At 561 nm excitation (with respect to NR excitation); the P-OPV-6+NR probe showed signals only in the red channel as a result of NR self-emission (no blue emission was found in blue channel).

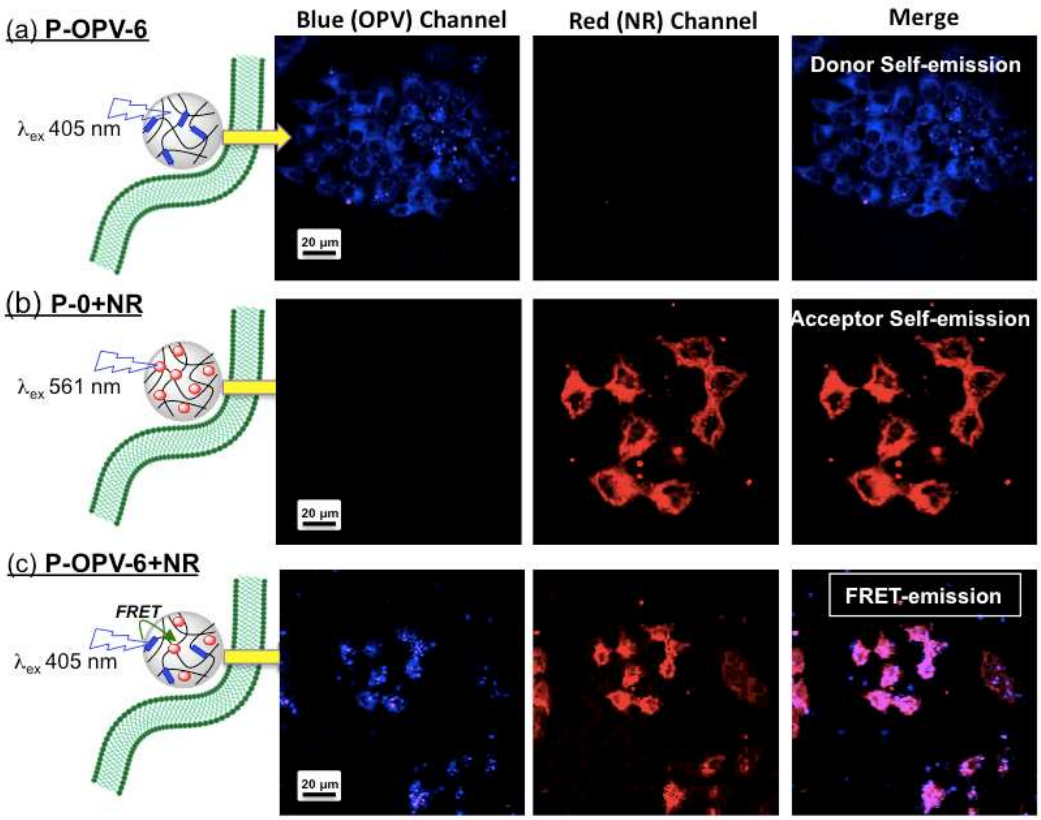

Figure 8. *Confocal microscope images in MCF 7 cells for P-OPV-6 (a), P-0+NR (b) and P-OPV-6+NR (c). The photoexcitation wavelengths for each panel are also given and the concentrations of the OPV chromophores in the polymer and NR are maintained as 0.1 O.D. and 0.03 O.D., respectively. The cells were incubated for 4h.*

The FRET between OPV donor and NR acceptor were also investigated in HeLa cell line. The selective excitation of OPV chromophore at 405 nm showed bright emission from OPV (at blue channel) and red-emission from NR (in red channel) followed by FRET process (see figure 9a). The merged images of the two showed the overlap of blue and red regions to give magenta colour which confirmed the presence of donor and acceptor at the same site in the HeLa cells. The WT-MEF followed identical trends similar to MCF 7 and HeLa cell lines; however the intensities were relatively low (see Figure 9b). The energy transfer from OPV chromophores to NR were further elaborated in FACS analysis as shown in figure 4e. For the same concentration of NR in P-0+NR, both HeLa and MCF7 cells cell lines showed NR emission intensities of 7700 and 4800, respectively (see figure 4e). Under identical conditions the P-OPV-6+NR showed, two fold increase in the NR emission intensities of 15000 and 9200 for HeLa and MCF 7 cell lines, respectively (see figure 4e). The 2-fold

increase in NR intensities in the presence of OPV donor was attributed to the occurrence of the FRET in the cells. Lysosomal tracker was employed in live cell CSLM imaging to identify the subcellular location of the polymer nanoparticles. The nascent blue luminescent P-OPV-6 nanoparticles, P-0+NR (non-luminescent polymer loaded with NR dye) and P-OPV-6+NR were incubated for 4 h in HeLa (cancer cell line) and WT-MEF (normal cell line). The CSLM images were recorded using 405 nm, 488 nm and 561 nm laser excitation sources for OPV, lysosomal tracker, and NR, respectively. The images were captured in the blue (410 – 460 nm), green (490 – 540 nm), and red (570 – 635 nm) channels, and they are shown in Figure 10 for HeLa cells.

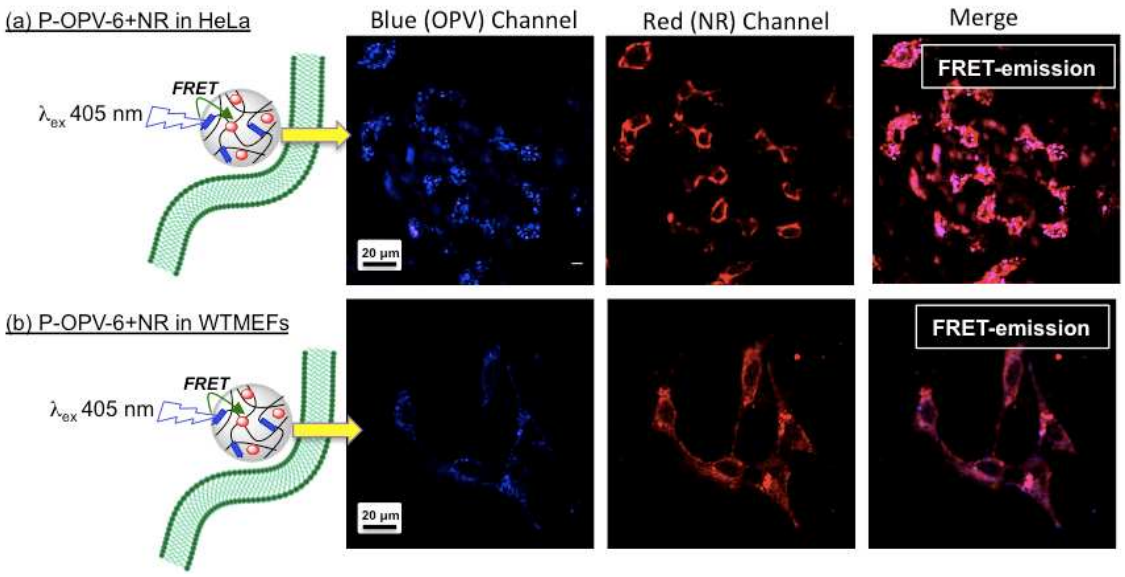

Figure 9. *Confocal microscope images in P-OPV-6+NR in HeLa (a) and WT-MEF (b) cell lines. The photoexcitation wavelengths for each panel are given and the concentrations of the OPV chromophores in the polymer and NR are maintained as 0.1 O.D. and 0.03 O.D., respectively. The cells were incubated for 4h.*

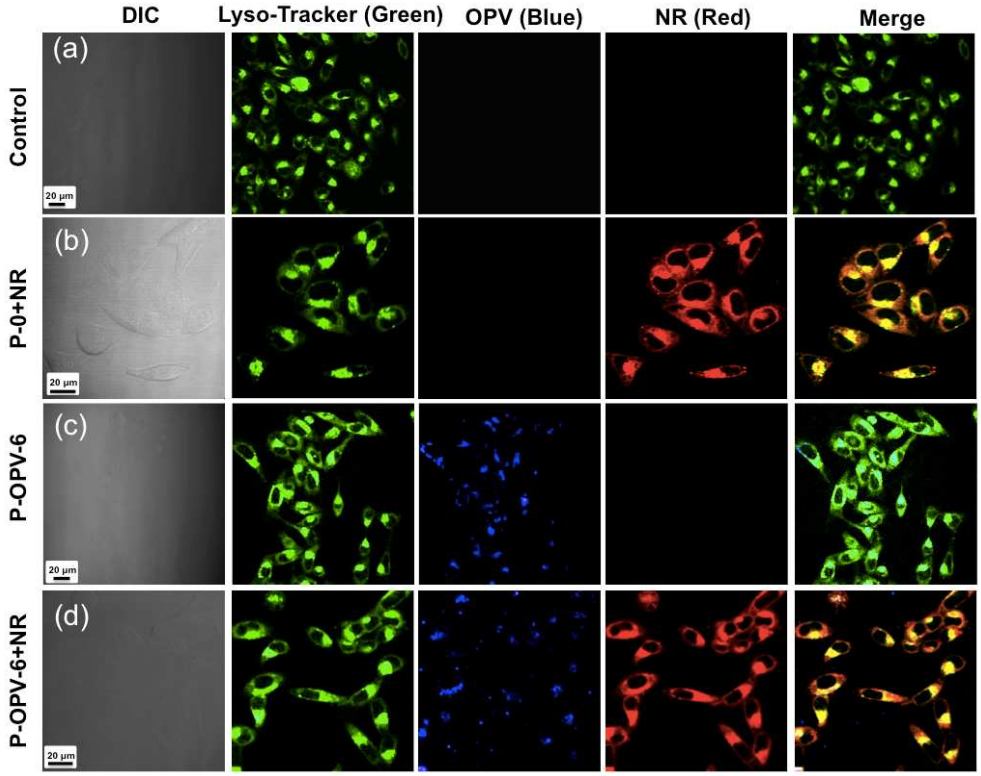

Figure 10. *Live cell confocal microscope images in HeLa cells for control (a), P-0+NR (b), P-OPV (c) and P-OPV-6+NR (d). The photoexcitation wavelengths for OPV, NR and Lyso tracker were 405, 561, 488 nm respectively, and the concentrations of the OPV chromophores in the polymer and NR are maintained as 0.1 O.D. and 0.03 O.D., respectively. The cells were incubated for 4h.*

The first row of panels in Figure 10a showed images of the cells incubated only with lysosomal tracker (without any nanoparticles). The lysosomes were clearly visible in the cytoplasm with bright green emission and no signals were observed in blue or red channels. The administration of lysosomal tracker stained the lysosomal compartments in the cells and the images appeared to be similar with literature report.[72] In Figure 10b, the NR loaded polymer nanoparticles P-0+NR exclusively showed bright red emission in the red channel. The merging of the P-0+NR nanoparticle image with the lysosomal tracker image confirmed that the P-0+NR nanoparticles were largely accumulated in the lysosomal compartments in the cytoplasm. The merged image was found to be yellow coloured followed by the combination of red and green emission together with NR in the lysosomal compartments inside the cells. In Figure 10c, the P-OPV-6 nanoparticles showed blue emission with respect to the OPV self-emission from the polymer . The closer observation of individual cells in the blue and green channel revealed the location of OPV polymer nanoparticles in the lysosomal

compartments. In figure 10d, the P-OPV-6+NR nanoparticle images exhibited dual blue and red emission from OPV and NR chromphores. The merged image showed the co-localization of both OPV and NR chromophores in the lysosomal compartments. Live cell imaging experiments in WT-MEF cell lines also revealed a similar trend for the OPV polymer and their NR loaded nanoparticles (see SF-18). This live cell imaging CSLM studies provided direct evidence for the cellular uptake of the L-aspartic acid polymer FRET nanoparticles and their transportation in the cytoplasm by the lysosomes. The susceptibility of the L-aspartic polyester nanoparticles biodegradation by the lysosomal-enzymes like esterase, chymotrypsin, and trypsin were already proven in Figure 6. Based on the live cell lysosomal tracker CSLM imaging (Figure 10) and enzyme-responsive biodegradation studies (Figure 6); it may be concluded that the custom designed L-aspartic polyester nanoparticles were readily taken up by the cells and transported-cum-digested in the lysosomal compartments in the cytoplasm of the cells. Though the concept was demonstrated here exclusively using OPV and NR FRET donor-acceptor pairs in L-aspartic acid polyester platform; the approach is not restricted to only these systems and in principle, it may be expanded to wide ranges of other L-amino acid resources.

Conclusion

To summarize new classes of π-conjugated luminescent L-amino acid based amphiphilic polyesters have been synthesized through solvent free melt condensation approach using L-aspartic acid monomers and custom designed OPV diol. Appropriate amphiphilicity was accomplished by carefully varying the compositions of OPV diol with hydrophilic triethylene glycol and hydrophobic 1,12-dodecane diol in one-pot melt condensation process. These polymers were shown to produce stable nanoparticles of < 200 nm in size under physiological conditions (pH = 7.4). They were found to be capable of loading hydrophobic water insoluble fluorophores like Nile Red. The polymer nano-aggregates were found to be highly sensitive to the environment and they exhibited one dimensional nano-fibrous morphology or spherical nanoparticles in organic or aqueous medium, respectively. Absorption, emission and time resolved fluorescent decay techniques were employed to study the occurrence of the FRET process between the OPV and NR chromphores in the nanoparticle domain. The OPV chromophores underwent strong aromatic π-π stacking in the aqueous medium and these aggregated conjugated domains were found to provide more than 75 % FRET overlap between OPV and NR. Detailed photophysical studies and energy calculations revealed that the newly designed polymer nanoparticle assembly

provided appropriate geometry for 88 % FRET efficiency having the Förster distance and distance between donor and acceptor as 39.24 Å and 28.13 Å, respectively. The nanoparticles were found to be biocompatible and non-toxic to cancer and normal cell lines. The aliphatic polyester backbone in the nanoparticle was found to be responsive to lysosome enzymes such as esterase, chymotrypsin, trypsin, and papain and GSH. These enzymes digested the polymer chains at the intracellular compartments, which make the FRET probe highly desirable for bio-imaging applications. Lyso-tracker assisted cellular uptake studies conformed that the nanoparticles co-localization in the lysosomal compartment in the cytoplasm. Confocal imaging with selective photo-excitation of FRET donor alone (OPV chromophore) produced bright blue-emission whereas bright-red emission was produced in the presence of FRET acceptor (NR chromophores) followed by the efficient FRET mechanism at the intracellular level. Merging of the blue and red emission produced magenta-emission owing to the greater colour-tunability of the FRET probe for bio-imaging applications. Currently efforts are being taken to apply the FRET concept and the synthetic methodology in L-amino acid to expand the approach to other systems in cancer research.

Supporting Information: ^{1}H-NMR, ^{13}C-NMR, MALDI/TOF TOF spectra, absorption and emission spectra, GPC chromatogram, DSC and TGA thermograms, polymer degradation data, FRET energy calculations, WT-MEF data using Lyso-tracker, cytotoxicity data for HeLa and WT-MEF cells, determination of dn/dc and molar extinction coefficient details are provided in supporting information. This material is available free of charge via the Internet at http://pubs.acs.org.

Acknowledgments: The authors thank research grant from Department of Science and Technology (DST) for the project SB/S1/OC-37/2013. Sonashree Saxena thanks IISER Pune for Ph.D research fellowship. She also thanks Mr. Narasimha Karnati for his valuable discussions and support during the synthesis of OPV diols. AFM facility is sponsored by the DST-FIST Project.

Author Information: Corresponding Author: Prof. Manickam Jayakannan [jayakannan@iiserpune.ac.in]. The authors declare no financial interest.

References:

1) Duan, X.; Liu, L.; Feng, F.; Wang, S. Cationic Conjugated Polymers for Optical Detection of DNA Methylation, Lesions, and Single Nucleotide Polymorphisms. *Acc. Chem. Res.* **2010**, *43*, 260-270.
2) Lv, F.; Qiu, T.; Liu, L.; Ying, J.; Wang, S. Recent Advances in Conjugated Polymer Materials for Disease Diagnosis. *Small*, **2016**, *6*, 696-705.
3) Li, C.; Liu, S. Polymeric Assemblies and Nanoparticles with Stimuli-responsive Fluorescence Emission Characteristics. *Chem. Commun.* **2012**, *48*, 3262-3278.
4) Li, K.; Liu, B. Water-soluble Conjugated Polymers as the Platform for Protein Sensors. *Polym. Chem.* **2010**, *1*, 252-259.
5) Huang, P.; Wang, D.; Su, Y.; Huang, W.; Zhou, Y.; Cui, D.; Zhu, X.; Yan, D. Combination of Small Molecule Prodrug and Nanodrug Delivery: Amphiphilic Drug-Drug Conjugate for Cancer Therapy. *J. Am. Chem. Soc*, **2014**, *136,* 11748-11756.
6) Dong, R.; Zhu, B.; Zhou, Y.; Yan, D.; Zhu, X. Breathing Vesicles with Jellyfish-like On-Off Switchable Fluorosence Behavior. *Angew Chem. Int. Edn*. **2012**, *51*, 11633-11637.
7) Huang, Y.; Wang, D.; Zhu, X.; Yan, D.; Chen, R. Synthesis and Therapeutic Applications of Biocompatible or Biodegradable Hyperbranched Polymers. *Polym. Chem.* **2015**, *6*, 2794-2812.
8) Fruhwirth, G. O.; Fernandes, L. P.; Weitsman, G.; Patel, G.; Kelleher, M.; Lawler, K.; Poland, S. P.; Brock, A.; Poland, S. P.; Matthews, D. R.; Kéri, G.; Barber, P. R.; Vojnovic, B.; Ameer-Beg, S. M.; Coolen, A. C. C.; Fraternali, F.; Ng, T. How Förster Resonance Energy Transfer Imaging Improves the Understanding of Protein Interaction Networks in Cancer Biology. *Chem Phys Chem*, **2011**, *12*, 442-461.
9) Sahoo, H. Förster Resonance Energy Transfer- A Spectroscopic Nanoruler: Principle and Applications. *J. Photochem. Photobiol. C: Photochem. Rev.* **2011**, *12*, 20-30.
10) Li, X.; Mu, J.; Liu, F.; Tan, E. W. P.; Khezri, B.; Webster, R. D.; Yeow, E. K. L.; Xing, B. Human Transport Protein Carrier for Controlled Photoactivation of Antitumor Prodrug and Real-Time Intracellular Tumor Imaging. *Bioconjugate Chem.* **2015**, *26*, 955-961.
11) Chen, J.; Zhong, W.; Tang, Y.; Wu, Z.; Li, Y.; Yi, P.; Jiang, J. Amphiphilic BODIPY-Based Photoswitchable Fluorescent Polymeric Nanoparticles for Rewritable Patterning and Dual-Color Cell Imaging. *Macromolecules* **2015**, *48*, 3500-3508.
12) Han, X.; Liu, De-E.; Wang, T.; Lu, H.; Ma, J.; Chen, Q.; Gao, H. Aggregation-Induced-Emissive Molecule Incorporated into Polymeric Nanoparticulate as FRET Donor for Observing Doxorubicin Delivery. *ACS Appl. Mater. Interfaces*, **2015**, *7*, 23760-23766.
13) Chen, H.; Kim, S.; Li, L.; Wang, S.; Park, K.; Cheng, J-X. Release of Hydrophobic Molecules from Polymer Micelles into Cell Membranes Revealed by Förster Resonance Energy Transfer Imaging. *Proc. Natl. Acad, Sci.* **2008**, *105*, 6596-6601.
14) Rajdev, P.; Basak, D.; Ghosh. S. Insights into Noncovalently Core Cross-Linked Block Copolymer Micelles by Fluorescence Resonance Energy Transfer Studies, *Macromolecules*, **2015**, *48,* 3360-3367.
15) Miyake-Stoner, S. J.; Miller, A. M.; Hammill, J. T.; Peeler, J. C.; Hess, K. R.; Mehl, R. A.; Brewer, S. H. Probing Protein Folding using Site-Specifically Encoded Unnatural Amino Acids as FRET Donors with Tryptophan. *Biochemistry*, **2009**, *48,* 5953-5962.
16) Maity, H.; Reddy, G. Folding of Protein L with Implications for Collapse in the Denatured State Ensemble. *J. Am. Chem. Soc*, **2016**, *138,* 2609-2616.

17) He, F.; Tang, Y.; Yu, M.; Feng, F.; An, L.; Sun, H.; Wang, S.; Li, Y.; Zhu, D.; Bazan, G. C. Quadruplex-to-Duplex Transition of G-Rich Oligonucleotides Probed by Cationic Water-Soluble Conjugated Polyelectrolytes. *J. Am. Chem. Soc.* **2006**,*128*, 6764-6765.
18) Lin, W.; Du, Y.; Zhu, Y.; Chen, X. A Cis-Membrane FRET-Based Method for Protein-Specific Imaging of Cell-Surface Glycans. *J. Am. Chem. Soc.* **2014**, *136*, 679-687.
19) Rana, S.; Elci, S. G.; Mout, R.; Singla, A. K.; Yazdani, M.; Bender, M.; Bajaj, A.; Saha, K.; Bunz, U. H. F.; Jirik, F. R.; Rotello, V. M. Ratiometric Array of Conjugated Polymers-Fluorescent Protein Provides a Robust Mammalian Cell Sensor. *J. Am. Chem. Soc.* **2016**, *138,* 4522-4529.
20) Cui, Q.; Wang, X.; Yang, Y.; Li, S.; Li, L.; Wang, S. Binding-Directed Energy Transfer of Conjugated Polymer Materials for Dual-Color Imaging of Cell Membrane. *Chem. Mater.* **2016***, 28*, 4661-4669.
21) Huang, Y.; Qiu, F.; Shen, L.; Chen, D.; Su, Y.; Yang, C.; Li, B.; Yan, D.; Zhu, X. Combining Two-Photon-Activated Fluorescence Resonance Energy Transfer and Near-Infrared Photothermal Effect of Unimolecular Micelles for Enhanced Photodynamic Therapy. *ACS Nano*, **2016**, *10*, 10489-10499.
22) He, F.; Ren, X.; Shen, X.; Xu, Q-H. Water-Soluble Conjugated Polymers for Amplification of One-and Two-Photon Properties of Photosensitizers. *Macromolecules,* **2011**, *44*, 5373-5380.
23) Senthilkumar, T.; Asha, S.K. Selective and Sensitive Sensing of Free Bilirubin in Human Serum Using Water-Soluble Polyfluorene as Fluorescent Probe. *Macromolecules,**2015**, 48*, 3449-3461.
24) Qiu, F.; Huang, Y.; Zhu, X. Fluorescent Unimolecular Conjugated Polymeric Micelles for Biomedical Applications. *Macromol. Chem. Phys*. **2016**, *217*, 266-283.
25) Ding, D.; Li, K.; Qin, W.; Zhan, R.; Hu, Y.; Liu, J.; Tang, B. Z.; Liu, B. Conjugated Polymer Amplified Far-Red/Near-Infrared Fluorescence from Nanoparticles with Aggregation-Induced Emission Characteristics for Targeted In Vivo Imaging. *Adv. Healthcare Mater,* **2013**¸*2*, 500-507.
26) Malik, A. H.; Hussain, S.; Iyar, P. K. Aggregation-Induced FRET via Polymer-Surfactant Complexation: A New Strategy for the Detection of Spermine. *Anal. Chem.*, **2016**, *88*, 7358-7364.
27) Zhu, C.; Yang, Q.; Liu, L.; Wang, S. Visual Optical Discrimination and Detection of Microbial Pathogens Based on Diverse Interactions of Conjugated Polyelectrolytes with Cells. *J. Mater. Chem*, **2011**, *21*, 7905-7912.
28) Wang, Y.; Li, S.; Feng, L.; Nie, C.; Liu, L.; Lv, F.; Wang, S. Fluorescence Ratiometric Assay Strategy for Chemical Transmitter of Living Cells Using H_2O_2-Sensitive Conjugated Polymers. *ACS Appl. Mater. Interfaces*. **2015**, *7*, 24110-24118.
29) Wang, S.; Gaylord, B. S.; Bazan, G. C. Fluorescein Provides a Resonance Gate for FRET from Conjugated Polymers to DNA Intercalated Dyes. *J. Am. Chem. Soc.* **2004**, *126,* 5446-5451.
30) Kahveci, Z.; Martínez-Tomé, M J.; Mallavia, R.; Mateo, C. R. Use of the Conjugated Polyelectolyte Poly{[9,9 bis(6'-N,N,N-trimethylammonium)hexyl]fluorene-phenylene} Bromide (HTMA-PFP) as a Fluorescent Membrane Marker. *Biomacromolecules,* **2013**, *14*, 1990-1998.
31) Huang, Y.; Qiu, F.; Chen, D.; Shen, L.; Xu, S.; Guo, D.; Su, Y.; Yan, D.; Zhu, X. Color-Convertible, Unimolecular, Micelle-based, Activatable Fluorescent Probe for Tumor-Specific Detection and Imaging *in vitro* and *in vivo*. *Small*, **2017**, DOI:10.1002/small.201604062.

32) Qiu, F.; Wang, D.; Wang, R.; Huan, X.; Tong, G.; Zhu, Q.; Yan, D.; Zhu, X. Temperature-Induced Emission Enhancement of Star Conjugated Copolymers with Poly(2-(dimethylamino)ethyl Methacrylate) Coronas for Detection of Bacteria. *Biomacromolecules,* **2013**, *14*, 1678-1686.

33) Kulkarni, B.; Surnar, B.; Jayakannan, M. Dual Functional Nanocarrier for Cellular Imaging and Drug Delivery in Cancer Cells Based on π-Conjugated Core and Biodegradable Polymer Arms**.** *Biomacromolecules,* **2016**, *17*, 1004-1016.

34) Endres, T.; Zheng, M.; Kılıç, A.; Turowska, A.; Beck-Broichsitter, M.; Renz, H.; Merkel, O. M.; Kissel, T. Amphiphilic Biodegradable PEG-PCL-PEI Triblock Copolymers for FRET-Capable *in vitro* and *in-vivo* Delivery of siRNA and Quantum Dots. *Mol. Pharmaceutics*, **2014**, *11*, 1273-1281.

35) Deming, T. J. Synthesis Polypeptides for Biomedical Applications. *Prog. Polym. Sci.* **2007**, *32*, 858-875.

36) Deming, T. J. Methodologies for Preparation of Synthetic Block Copolypeptides: Materials with Future Promise in Drug Delivery. *Adv. Drug Delivery. Rev*. **2002**, *54*, 1145-1155.

37) Osada, K.; Kataoka, K. Drug and Gene Delivery Based on Supramolecular Assembly of PEG-polypeptide Hybrid Block Copolymers. *Adv. Polym. Sci.* **2006**, *202*, 113-153.

38) Sun, H.; Meng, F.; Dias, A. A.; Hendriks, M.; Feijen, J.; Zhong, Z. α-Amino Acid Containing Degradable Polymers as Functional Biomaterials: Rational Design, Synthetic Pathway, and Biomedical Applications. *Biomacromolecules*, **2011**, *12*, 1937-1955.

39) Sun, H.; Cheng, R.; Deng, C.; Meng, F.; Dias, A. A.; Hendriks, M.; Feijen, J.; Zhong, Z. Enzymatically and Reductively Degradable α-amino Acid-based Poly(ester amide)s: Synthesis, Cell Compatibility, and Intra Cellular Anti Cancer Drug Delivery. *Biomacromolecules*, **2015**, *16*, 597-605.

40) Deng, M.; Wu, J.; Reinhart-King, C. A.; Chu, C. C. Synthesis and Characterization of Biodegradable Poly(ester amide)s with Pendant Amine Functional Groups and In Vitro Cellular Response. *Biomacromolecules*, **2009**, *10*, 3037-3047.

41) Fonseca, A. C.; Gil, M. H.;Simões P. N. Biodegradable Poly(ester amide)s- A Remarkable Opportunity for the Biomedical Area: Review on the Synthesis, Characterization and Applications. *Prog. Polym. Sci.* **2014**, *39*, 1291-1311.

42) Yin, Q.; Yin, L.; Wang, H.; Cheng, J. Synthesis and Biomedical Applications of Functional Poly(α-hydroxy acids) via Ring-Opening Polymerization of *O*-Carboxyanhydrides *Acc. Chem. Res.* **2005**, *48*, 1777-1787.

43) Magno, M. H. R.; Kim, J.; Srinivasan, A.; McBride, S.; Bolikal, D.; Darr, A.; Hollinger, J, O.; Kohn, J. Synthesis, Degradation and Biocompatibility of Tyrosine-derived Polycarbonate Scaffolds. *J. Mater. Chem*. **2010**, *20*, 8885-8893.

44) Sheihet, L.; Piotrowska, K.; Dubin, R. A.; Kohn, J.; Devore, D. Effect of Tyrosine-derived Triblocks Copolymer Compositions on Nanosphere Self-Assembly and Drug Delivery. *Biomacromolecules*, **2007**, *8*, 998-1003.

45) Aamer, K. A.; Genson, K. L.; Kohn, J.; Becker, M. L. Impact of Polymer-bound Iodine on Fibronectin Adsorption and Osteoblast Cell Morphology in Radiopaque Medical Polymers: Tyrosine-derived Polycarbonate Blends as a Model System. *Biomacromolecules*, **2009**, *10*, 2418-2426.

46) Tziampazis, E.; Kohn, J.; Moghe, P. V. PEG-variant Biomaterials as Selectively Adhesive Protein Templates: Model Surfaces for Controlled Cell Adhesion and Migration. *Biomaterials*, **2000**, *21*, 511-520.

47) Shpaisman, N.; Sheihet, L.; Bushman, J.; Winters, J.; Kohn, J. One-step Synthesis of Biodegradable Curcumin-derived Hydrogels as Potential Soft Tissue Fillers after Breast Cancer Surgery. *Biomacromolecules*, **2012**, *13*, 2279-2286.
48) Wu, J.; Zhao, L.; Xu, X.; Bertrand, N.; Choi, W.; Yameen, B.; Shi, J.; Shah, V.; Mulvale, M.; MacLean, J. L.; Farokhzad, O. C. Hydrophobic Cysteine Poly(disulfide)-based Redox-Hypersensitive Nanoparticle Platform for Cancer Theranostics. *Angew. Chem. Int. Ed.* **2015**, *54*, 9218-9223.
49) Lu, W.; Wang, X.; Cheng, R.; Deng, C.; Meng, F.; Zhong, Z. Biocompatible and Bioreducible Micelles Fabricated from Novel α-Amino Acid-based Poly(disulfide urethane)s: Design, Synthesis and Triggered Doxorubicin Release. *Polym. Chem*. **2015**, *6*, 6001-6010.
50) Anantharaj S.; Jayakannan, M. Polymers from Amino Acids: Development of Dual Ester-urethane Melt Condensation Approach and Mechanistic Aspects. *Biomacromolecules,* **2012**, *13*, 2446-2455.
51) Anantharaj S.; Jayakannan, M. Catalyst and Temperature Driven Melt Polycondensation Reaction for Helical Poly(ester-urethane)s Based on Natural L-Amino acids. *J. Polym. Sci., Polym Chem.* **2016**, *54*, 1065-1077.
52) Aluri, R.; and Jayakannan, M. One-pot Two Polymers: ABB' Melt Polycondensation for Linear Polyesters and Hyperbranched Poly(ester-urethane)s Based on Natural L-Amino acids. *Polym. Chem*. **2015**, *6*, 4641-4649.
53) Anantharaj S.; Jayakannan, M. Melt Polycondensation Approach for Reduction Degradable Helical Polyester Based on L-Cystine. *J. Polym. Sci., Polym Chem.* **2016**, *54*, 2864-2875.
54) Anantharaj S.; Jayakannan, M. Amyloid-like Hierarchical Helical Fibrils and Conformational Reversibility in Functional Polyesters Based on L-Amino acids. *Biomacromolecules,* **2015**, *16*, 1009-1020.
55) Saxena, S.; Jayakannan, Enzyme and pH Dual Responsive L-Amino Acid Based Biodegradable Polymer Nanocarrier for Multidrug Delivery to Cancer Cells. M. *J. Polym. Sci., Polym Chem.* **2016**, *54*, 3279-3293.
56) Aluri, R.; Jayakannan, M. Development of L-Tyrosine-Based Enzyme-Responsive Amphiphilic Poly(ester-urethane) Nanocarriers for Multiple Drug Delivery to Cancer Cells. *Biomacromolecules,* **2017**, *18*, 189-200.
57) Narasimha, K.; Jayakannan, M. Color-Tunable Amphiphilic Segmented π-Conjugated Polymer Nano-Assemblies and their Bioimaging in Cancer Cells. *Macromolecules,* **2016**, *49*, 4102-4114.
58) Amrutha, S. R.; Jayakannan, M. Structure Control of π-Conjugated Polymers for Enhanced Solid State Luminescence: Synthesis, Liquid Crystalline and Photophysical Properties of New Bulky Poly (p-phenylenevinylene)s and Oligo-(Phenylenevinylene)s Bearing Tricyclodecane Pendants, *Macromolecules*, **2007,** *40, 2380 – 2391.*
59) Goel, M.; Narasimha, K.; Jayakannan, M. Helical Self-Assemblies of Segmented Poly(phenylenevinylene)s and Their Hierarchical Donor–Acceptor Complexes. *Macromolecules*, **2014**, *47*, 2592-2603.
60) Rautio, J.; Kumpulainen, H.; Heimbach, T.; Oliyai, R.; Oh, D.; Järvinen, T.; Savolainen, J. Produgs: Design and Clinical Applications. *Nat. Rev.* **2008,** *7*, 255–270.
61) Pramod, P. S.; Shah, R.; Sonali, C.; Balasubramanian, N.; Jayakannan, M. Polysaccharide Nano-vesicular Multidrug Carrier for Synergistic Killing of Cancer Cells, *Nanoscale*, **2014**, *6*, 11841- 11855.

62) Anilkumar, P; Jayakannan, M. Fluorescent Tagged Probing Agent and Structure Directing Amphiphilic Molecular Design for Polyaniline Nano-materials via Self-assembly Process. *J. Phys. Chem. C*. **2007,** *111***,** 3591-3600.

63) Rychter, P.; Kawalec, M.; Sobota, M.; Kurcok, P.; Kowalczuk, M. Study of Aliphatic-Aromatic Copolyester Degradation in Sandy Soil and its Ecotoxicological Impact. *Biomacromolecules,* **2010**, *11*, 839-847.

64) Karpenko, I. A.; Klymchenko, A. S.; Gioria, S.; Kreder, R.; Shulov, I.; Villa, P.; Mely, Y.; Hibert, M.; Bonnet, D. Squaraine as a Bright, Stable and Environment Sensitive Far-Red Label for Receptor-Specific Cellular Imaging. *Chem. Commun*. **2015**, *51*, 2960-2963.

65) Datta, A.; Mandal, D.; Pal, S. K.; Bhattacharyya, K. Intramolecular Charge Transfer Processes in Confined Systems. Nile Red in Reverse Micelles. *J. Phys. Chem. B.* **1997**, *101*, 10221-10225.

66) Ghaffar, A.; Draaisma, G. J. J.; Mihov, G.; Dias, A. A.; Schoenmakers, P. J.; Wal, S. Van der. Monitoring the In Vitro Enzyme-Mediated Degradation of Degradable Poly(ester amide) for Controlled Drug Delivery by LC-ToF-MS. *Biomacromolecules,* **2011**, *12*, 3243-3251.

67) Woodruff, M. A.; Hutmacher, D. W. The Return of a Forgotten Polymer-Polycaprolactone in the 21st Century. *Progress in Polymer Science* **2010**, *35*, 1217-1256.

68) Malhotra, M.; Surnar, B.; Jayakannan, M. Polymer Topology Driven Enzymatic Biodegradation in Polycaprolactone Block and Random Copolymer Architectures for Drug Delivery to Cancer Cells. *Macromolecules,* **2016**, *49*, 8098-8112.

69) Surnar, B.; Jayakannan, M. Stimuli-Responsive Poly(caprolactone) Vesicles for Dual Drug Delivery Under the Gastrointestinal Tract. *Biomacromolecules,* **2013**, *14*, 4377-4387.

70) Wang, J.; Sun, X.; Mao, W.; Sun, W.; Tang, J.; Sui, M.; Shen, Y.; Gu, Z. Tumor Redox Heterogeneity-Responsive Prodrug Nanocapsules for Cancer Chemotherapy. *Adv. Mater.* **2013**, *25*, 3670-3676.

71) Ohya, Y.; Takamido, S.; Nagahama, K.; Ouchi, T.; Katoono, R.; Yui, N. Polyrotaxane Composed of Poly-L-Lactide and α-Cyclodextrin Exhibiting Protease-Triggered Hydrolysis. *Biomacromolecules,* **2009**, *10*, 2261-2267.

72) Jia, X.; Chen, Q.; Yang, Y.; Tang, Y.; Wang, R.; Xu, Y.; Zhu, W.; Qian, X. FRET-Based Mito-Specific Fluorescent Probe For Ratiometric Detection and Imaging of Endogenous Peroxynitrite: Dyad of Cy3 and Cy5. *J. Am. Chem. Soc.* **2016**, *138,* 10778-10781.

Table of Contents

π-Conjugate Fluorophore-tagged and Enzyme-responsive L-Amino acid Polymer Nano-carrier and their Colour-tunable Intracellular FRET Probe in Cancer Cells.

Sonashree Saxena and Manickam Jayakannan*